

Gravitational and Gravitoscalar Thermodynamics

Shoichiro Miyashita*

Department of Physics, Waseda University, Okubo 3-4-1, Shinjuku, Tokyo 169-8555, Japan

Abstract

Gravitational thermodynamics and gravitoscalar thermodynamics with $S^2 \times \mathbb{R}$ boundary geometry are investigated through the partition function, assuming that all Euclidean saddle point geometries contribute to the path integral and dominant ones are in the $B^3 \times S^1$ or $S^2 \times Disc$ topology sector. In the first part, I concentrate on the purely gravitational case with or without a cosmological constant and show there exists a new type of saddle point geometry, which I call the “bag of gold(BG) instanton,” only for the $\Lambda > 0$ case. Because of this existence, thermodynamical stability of the system and the entropy bound are absent for $\Lambda > 0$, these being universal properties for $\Lambda \leq 0$. In the second part, I investigate the thermodynamical properties of a gravity-scalar system with a φ^2 potential. I show that when $\Lambda \leq 0$ and the boundary value of scalar field J_φ is below some value, then the entropy bound and thermodynamical stability do exist. When either condition on the parameters does not hold, however, thermodynamical stability is (partially) broken. The properties of the system and the relation between BG instantons and the breakdown are discussed in detail.

*e-mail address : s-miyashita@at.aoni.waseda.jp

Contents

1	Introduction	3
2	Partition functions for gravity-scalar system	4
3	Gravitational thermodynamics	5
3.1	$\Lambda = 0$	6
3.2	$\Lambda < 0$	8
3.3	$\Lambda > 0$	11
3.3.1	$0 < \Lambda < \frac{3}{r_b^2}$	12
3.3.2	$\frac{3}{r_b^2} \leq \Lambda$	16
4	Gravitoscalar thermodynamics with a simple potential	16
4.1	Conditions for the existence of saddle points	17
4.2	Thermodynamic potentials and thermodynamic properties	24
4.2.1	$-\infty < \Lambda \leq 0$	26
4.2.2	$0 < \Lambda \leq \frac{1}{r_b^2}$	28
4.2.3	$\frac{1}{r_b^2} < \Lambda \leq \frac{3}{r_b^2}$	31
4.2.4	$\frac{3}{r_b^2} < \Lambda < \infty$	31
5	Discussion	31
A	Numerical solutions in the gravity-scalar system	33
A.1	Euclidean soliton	35
A.2	Euclidean BH	35
A.3	BG instanton	39
A.4	PL type solution	39

1 Introduction

At the moment, we do not know how to track the fine-grained dynamics of quantum gravity. However, one promising thing is that gravity would reach (thermal) equilibrium as do usual systems with many degrees of freedom. The outset is the discovery of black hole (BH) thermodynamics [1, 2], which states that BHs can be treated as if they have temperature and entropy and obey the thermodynamical laws. To uncover this mysterious phenomena, Gibbons and Hawking tried to derive these laws by a statistical treatment; that is, they defined the partition function by the path integral of gravity, and actually re-derived the thermodynamical laws [3]. Indeed, the system they considered is thermodynamically unstable in the sense that it has a negative heat capacity. However, what they considered is the partition function of gravity (not of BHs) with the asymptotically flat boundary condition. Later, Hawking and Page introduced a negative cosmological constant and changed the boundary condition to the asymptotically Anti-de Sitter (AdS) one [4]. They showed that the system is thermodynamically stable and exhibits a phase transition, which is now called the Hawking–Page phase transition. Therefore, gravity actually thermalizes and we could elucidate the coarse-grained dynamics of quantum gravity through the partition function.

For pure gravity, the thermodynamical properties of the following four cases are known in the literature:

- $\Lambda = 0$, asymptotically flat boundary condition [3]
- $\Lambda < 0$, asymptotically AdS boundary condition [4]
- $\Lambda = 0$, finite radius $S^2 \times \mathbb{R}$ boundary condition [5]
- $\Lambda < 0$, finite radius $S^2 \times \mathbb{R}$ boundary condition [6]

The first one, as mentioned above, is thermodynamically unstable. The second, third, and fourth ones share qualitatively the same properties: they are thermodynamically stable and exhibit a Hawking–Page phase transition. In this paper, after reviewing the third and fourth cases, I investigate the case of $\Lambda > 0$ and finite radius $S^2 \times \mathbb{R}$ boundary condition to know completely the thermodynamical properties of pure gravity. After that, as a simple extension, I consider a gravity-scalar system with a φ^2 potential to obtain intuitions about the coarse-grained dynamics/properties of quantum gravity when it couples to matter fields. In addition, in light of holography [7, 8], these will be some clues to specify what class of quantum field theory corresponds to gravity when it is not with the asymptotically AdS boundary condition.

The paper is organized as follows. In section 2, the path integral representation of the partition function of a gravity(-scalar) system is briefly reviewed and I also mention the minisuperspace used in this paper. In section 3, gravitational thermodynamics with or without a cosmological constant is discussed. Subsections 3.1 and 3.2 are devoted to reviewing the thermodynamics of gravity with $\Lambda \leq 0$ and finite radius $S^2 \times \mathbb{R}$ boundary condition. In subsection 3.3, thermodynamics with $\Lambda > 0$ and finite radius $S^2 \times \mathbb{R}$ boundary condition is investigated. I show that there exists a new type of Euclidean saddle point geometry that makes the thermodynamical properties drastically different from those in the $\Lambda \leq 0$ cases. In section 4, I introduce a scalar field with a φ^2 potential into the system and investigate its thermodynamical properties. Before discussing thermodynamical properties, in subsection 4.1 I show the conditions for the existence of saddle points. In subsection 4.2, thermodynamical properties are discussed. In the system, in order to obtain saddle point geometries, we have to employ numerical calculation. The detail of the calculation and some examples of saddle points are shown in Appendix A. Section 5 is devoted to a summary and discussions.

2 Partition functions for gravity-scalar system

The partition function of canonical ensembles for gravity may be obtained by Euclidean gravitational path integral, which includes the summation of manifold topology \mathcal{M} [3, 5]:

$$Z_c = \sum_{\mathcal{M}} \int \mathcal{D}\mathbf{g} e^{-I_c^E[\mathbf{g}]} \quad (2.1)$$

$I_c^E[\mathbf{g}]$ is the Euclidean gravitational action functional for canonical ensembles, that is, for Dirichlet type boundary conditions:

$$I_c^E[\mathbf{g}] = \frac{-1}{16\pi G} \int_{\mathcal{M}} d^4x \sqrt{g} (\mathcal{R} - 2\Lambda) + \frac{-1}{8\pi G} \int_{\partial\mathcal{M}} d^3y \sqrt{\gamma} (\Theta - \Theta_{sub}) \quad (2.2)$$

Θ is the extrinsic curvature of $\partial\mathcal{M}$ and Θ_{sub} is the subtraction term needed for regularization in case on-shell actions diverge. Although it is not necessary for the analysis in this paper, for convenience I use it for setting the (free) energy of the ground states to zero. I adopt the Mann counterterm [9] for the subtraction term, which has been shown to work well for the purpose for spacetimes with $S^2 \times \mathbb{R}$ boundary geometry [10, 11]:¹

$$\Theta_{sub} = \Theta_{Mann}(\gamma) = \sqrt{2\mathcal{R}^{(3)} - \frac{4}{3}\Lambda} \quad (2.3)$$

I concentrate only on the case that the boundary manifold has $S^2 \times S^1$ topology and whose geometry is the product of a geometric 2-sphere and a circle. This corresponds to the partition function of thermal equilibrium of a quantum spacetime whose boundary geometry is $S^2 \times \mathbb{R}$. Suppose the dominant paths come from the saddle points of relatively simple topology sectors, say $S^2 \times D(isc)$ and $B^3 \times S^1$; then, Eq. (2.1) can be approximated

$$Z_c(\beta, A; \Lambda) \simeq \sum_{\text{saddles of } S^2 \times D} e^{-I_c^{E,os}} + \sum_{\text{saddles of } B^3 \times S^1} e^{-I_c^{E,os}} \quad (2.4)$$

“os” represents on-shell. Additionally, I assume the dominant paths are in a simple minisuperspace,² a class of 4-dim. metrics whose member takes the following form:

$$\mathbf{g}(x) = f(r)d\tau^2 + \frac{N^2}{f(r)}dr^2 + R(r)^2(d\theta^2 + \sin^2\theta d\phi^2) \quad (2.5)$$

In this setup, the canonical partition function and microcanonical partition function of finite boundary volume were investigated previously in [5, 12, 13, 14, 15, 16, 17, 18]. I will review $\Lambda \leq 0$ cases and give some new results on the $\Lambda > 0$ case in section 3.

As long as we concentrate only on saddle points, we can fix the gauge as

$$\mathbf{g}(x) = f(r)d\tau^2 + \frac{1}{f(r)}dr^2 + r^2(d\theta^2 + \sin^2\theta d\phi^2) . \quad (2.6)$$

¹Precisely, in [10], the Mann counterterm and its straightforward generalizations were shown to set the ground state energy to zero for spacetimes with $S^{d-2} \times \mathbb{R}$ boundary geometry.

²Originally, superspace is the configuration space of general relativity and minisuperspace means some subset of it. I will abuse the word “minisuperspace” in the context of gravitational path integral.

I will use r_b for the boundary value of the r coordinate that satisfies $A = 4\pi r_b^2$. Energy can be defined by the Brown–York tensor [19] and, according to my choice of counterterm, it is given by

$$E = \frac{r_b}{G} \left[\sqrt{1 - \frac{\Lambda}{3} r_b^2} - \sqrt{f(r_b)} \right] \quad (2.7)$$

when the r coordinate decreases from the boundary $r = r_b$ and

$$E = \frac{r_b}{G} \left[\sqrt{1 - \frac{\Lambda}{3} r_b^2} + \sqrt{f(r_b)} \right] \quad (2.8)$$

when it increases from the boundary.

The objective of this paper is to investigate the thermodynamical properties of a gravity-scalar system. Especially, I will consider a scalar field with a φ^2 potential. The action functional I will use in section 4 is

$$I_c^E[\mathbf{g}, \varphi] = I_c^E[\mathbf{g}] + \int_{\mathcal{M}} d^4x \sqrt{g} \left[\frac{1}{2} g^{\mu\nu} \partial_\mu \varphi \partial_\nu \varphi + \frac{1}{2} M^2 \varphi^2 \right] \quad (2.9)$$

where M^2 is the mass of the scalar field and $\frac{\Lambda}{8\pi G}$ can be considered as the minimum of the potential $V(\varphi) \equiv \frac{\Lambda}{8\pi G} + \frac{1}{2} M^2 \varphi^2$. The corresponding canonical partition function of gravitoscalar thermal equilibrium is given by³

$$Z_c(\beta, A; \Lambda, M, J_\varphi) = \sum_{\mathcal{M}} \int \mathcal{D}\mathbf{g} \mathcal{D}\varphi e^{-I_c^E[\mathbf{g}, \varphi]} \quad (2.10)$$

where J_φ is the boundary value of φ . I will approximate this by saddle points in a minisuperspace

$$\mathbf{g}(x) = f(r) e^{-2\delta(r)} d\tau^2 + \frac{1}{f(r)} dr^2 + r^2 (d\theta^2 + \sin^2 \theta d\phi^2), \quad (2.11)$$

$$\varphi(x) = \varphi(r). \quad (2.12)$$

Throughout this paper, I assume all Euclidean saddle points in the minisuperspace contribute to the path integral.⁴

3 Gravitational thermodynamics

In this section, I firstly review the thermodynamical properties of gravity alone without or with a negative cosmological constant in subsections 3.1 and 3.2. These are quantitatively different of course but qualitatively the same. We will see this is not the case for a positive cosmological constant in subsection 3.3.

³Although I employ Dirichlet type boundary conditions to the Euclidean path integral of the gravity-scalar system, it still represents the canonical partition function. We can confirm $I_c^E \simeq \beta E - S$ at the saddle points (4.2) by using the equation of motion (A.4). This fact is in contrast to the case of the Einstein-Maxwell system, where $I_c^E \simeq \beta E - S - \beta \mu Q$ at the saddle points when we employ Dirichlet type boundary conditions [20] (here, μ is the electric potential and Q is the electric charge).

⁴This assumption is not so trivial because there exists the contour problem in the Euclidean path integral of gravity [21, 22]. I will mention it in the final section.

3.1 $\Lambda = 0$

As is well known, Gibbons and Hawking showed that gravitational thermodynamics in asymptotically flat spacetime is *ill-defined* in the sense that quantum spacetimes with the asymptotics never realize thermal equilibrium states [3]. After the work by Hawking and Page [4] that claimed that those with AdS asymptotics do reach thermal equilibrium, York claimed that quantum spacetimes without Λ having a time-like boundary with finite spatial volume also reach thermal equilibrium [5]. He considered a gravitational partition function of a quantum spacetime with an $S^2 \times \mathbb{R}$ Lorentzian boundary geometry, which may be given by summing over Euclidean geometries with an $S^2 \times S^1$ Euclidean boundary geometry. It was approximated by contributions from the following saddle points

$$\mathbf{g}(x) = f(r)d\tau^2 + \frac{1}{f(r)}dr^2 + r^2(d\theta^2 + \sin^2\theta d\phi^2) \quad (3.1)$$

$$f(r) = 1 - \frac{2Gm}{r} \quad \text{for } S^2 \times D \text{ topology} \quad (3.2)$$

$$f(r) = 1 \quad \text{for } B^3 \times S^1 \text{ topology} \quad (3.3)$$

where the coordinate ranges of r and τ , $[2Gm, r_b]$ and $[0, \beta_0]$, and the mass parameter m should be chosen appropriately for given β and A . Namely, they must satisfy

$$\frac{4\pi}{f'(2Gm)} = \beta_0, \quad \sqrt{f(r_b)}\beta_0 = \beta, \quad 4\pi r_b^2 = A \quad \text{for } S^2 \times D \text{ topology} \quad (3.4)$$

$$M = 0, \quad \beta_0 = \beta, \quad 4\pi r_b^2 = A \quad \text{for } B^3 \times S^1 \text{ topology} \quad (3.5)$$

where the first condition for $S^2 \times D$ topology is for a conical singularity not to appear at the center of D , and the second and third for both topologies are for matching to boundary conditions. These geometries are shown in Fig. 1. The resulting saddle point contributions are

$$\text{Branch 1A :} \quad 1 \quad \text{for any value of } \beta \quad (3.6)$$

$$\text{Branch 1B :} \quad \exp \left[-\frac{1}{G} \left(\frac{3}{16\pi} \beta_0^-(\beta, r_b)^2 - r_b \beta_0^-(\beta, r_b) + r_b \beta \right) \right] \quad \text{for } \beta \leq \frac{8\pi r_b}{3\sqrt{3}} \quad (3.7)$$

$$\text{Branch 1C :} \quad \exp \left[-\frac{1}{G} \left(\frac{3}{16\pi} \beta_0^+(\beta, r_b)^2 - r_b \beta_0^+(\beta, r_b) + r_b \beta \right) \right] \quad \text{for } \beta \leq \frac{8\pi r_b}{3\sqrt{3}} \quad (3.8)$$

where β_0^+ and β_0^- are the positive roots of

$$\beta_0^3 - 4\pi r_b \beta_0^2 + 4\pi r_b \beta^2 = 0 \quad (3.9)$$

for $\beta \leq \frac{8\pi r_b}{3\sqrt{3}}$, and β_0^+ is defined to be the larger one and β_0^- is the smaller one.⁵ Equation (3.9) comes from the first and second conditions for $S^2 \times D$ topology (3.4). Branch 1A is from the $B^3 \times S^1$ topology sector and branches 1B and 1C are from the $S^2 \times D$ topology sector. The behaviors of

⁵Equation (3.9) has one negative root, and two complex roots for $\beta > \frac{8\pi r_b}{3\sqrt{3}}$ and two positive roots for $\beta < \frac{8\pi r_b}{3\sqrt{3}}$. Although I ignore the former case, it will be important when we consider the integration contour of the path integral, and it is essentially the source of the difficulty for the well-definedness of the canonical partition function [14].

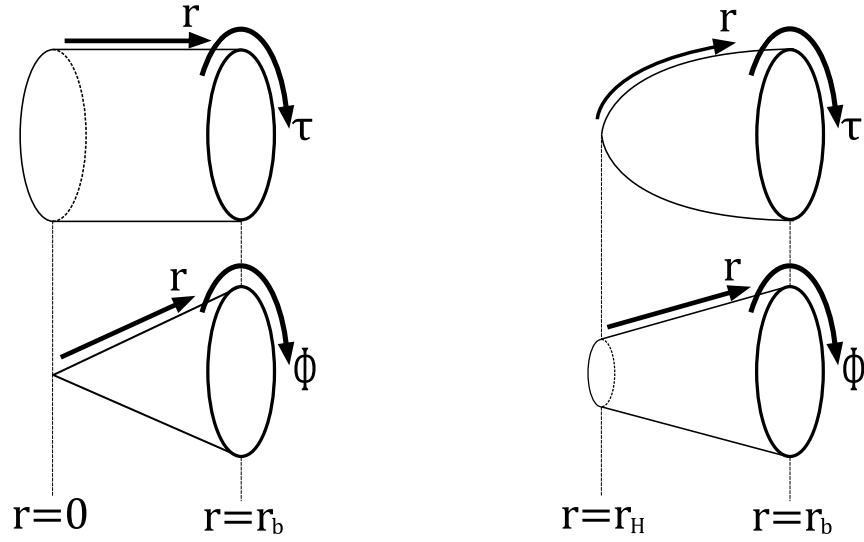


Figure 1: **(Left)** Saddle point geometry of $B^3 \times S^1$ topology. The upper is the r - τ section and the lower is the r - ϕ section. Note that the r - ϕ section is just a disc D , that is, $2(3)$ -ball $B^{2(3)}$, and is not conic as the figure shows, and especially there is no singularity at the center $r = 0$. **(Right)** Saddle point geometry of $S^2 \times D$ topology (Euclidean BH). The r - τ section is smoothly capped at $r = r_H$.

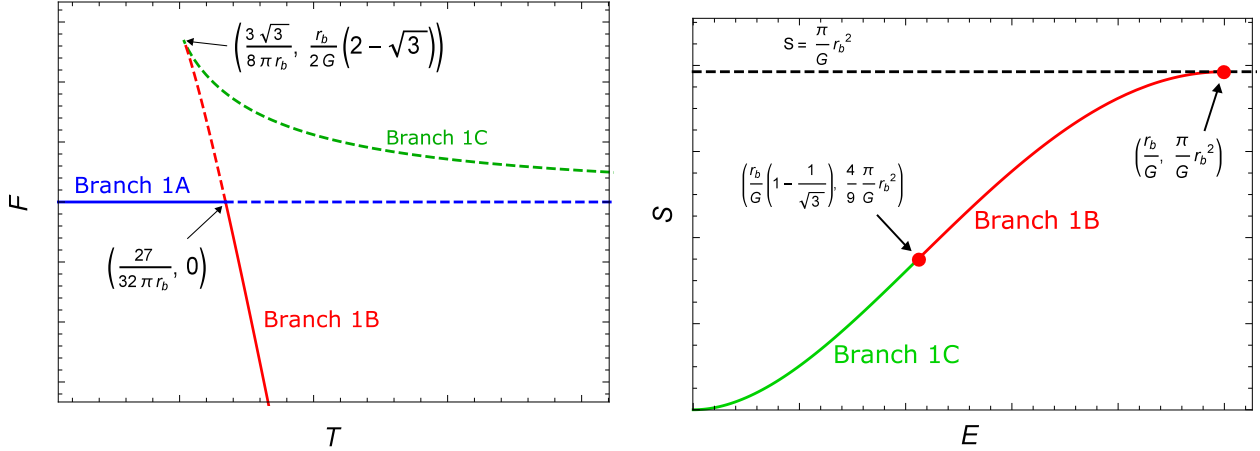


Figure 2: **(Left)** Qualitative behavior of free energies of saddles 1A, 1B, and 1C. The portion that does not give dominant contribution is dashed. **(Right)** Qualitative behavior of entropy as the function of energy. The maximum energy is $\frac{r_b}{G}$ and the maximum entropy is $\frac{\pi}{G} r_b^2$.

the corresponding free energies against temperature are shown in Fig. 2. Branch 1A is dominant when $T \in \left[0, \frac{27}{32\pi r_b}\right]$ and branch 1B is when $T \in \left[\frac{27}{32\pi r_b}, \infty\right)$. The former may be interpreted as flat spacetime with thermal radiations and the latter as BH spacetime (with thermal radiations). Branch 1C is never dominant, its heat capacity computed from its free energy is always negative, and it will be the only BH branch when we take the limit $r_b \rightarrow \infty$, which implies non-existence of gravitational thermal equilibrium in asymptotically flat spacetime.

We can also plot the E - S diagram. The rightmost endpoint of 1B is located at $\left(\frac{r_b}{G}, \frac{\pi}{G}r_b^2\right)$, which corresponds to the infinite temperature state in the canonical ensembles. We can interpret this diagram in two ways. One way is to interpret it as simply representing the energy and entropy of thermal equilibrium states that may be described by the canonical ensembles. In that case, only the information of some restricted region of 1B is important since the other regions of 1B and 1C are fictitious in the sense that they are not realized in thermal equilibrium. The other way is to think of this microcanonical ensemble as describing equilibrium states that are realized when the system is isolated. In any case, there exists maximum energy and entropy. Especially, entropy is always bounded by the entropy bound and saturated at the maximum energy.⁶

3.2 $\Lambda < 0$

Asymptotically AdS spacetime is the first example where there exists gravitational thermal equilibrium, shown by Hawking and Page [4]. After their work and York's work, which I reviewed in the previous subsection, Brown et al. generalized York's work to the case with negative Λ and with a time-like boundary of finite boundary volume [6]. The saddle points they considered are

$$g(x) = f(r)d\tau^2 + \frac{1}{f(r)}dr^2 + r^2(d\theta^2 + \sin^2\theta d\phi^2) \quad (3.10)$$

$$f(r) = 1 - \frac{\Lambda}{3}r^2 \quad \text{for } B^3 \times S^1 \text{ topology} \quad (3.11)$$

$$f(r) = 1 - \frac{2Gm}{r} - \frac{\Lambda}{3}r^2 \quad \text{for } S^2 \times D \text{ topology} \quad (3.12)$$

As before, the coordinate ranges of r and τ , $[r_H, r_b]$ and $[0, \beta_0]$, and the mass parameter m should be chosen appropriately for given β and A . They must satisfy

$$f(r_H) = 0, \quad \frac{4\pi}{f'(r_H)} = \beta_0, \quad \sqrt{f(r_b)}\beta_0 = \beta, \quad 4\pi r_b^2 = A \quad \text{for } S^2 \times D \text{ topology} \quad (3.13)$$

$$r_H = 0, \quad \sqrt{f(r_b)}\beta_0 = \beta, \quad 4\pi r_b^2 = A \quad \text{for } B^3 \times S^1 \text{ topology} \quad (3.14)$$

Qualitatively, these geometries are the same as those of the $\Lambda = 0$ case (Fig. 1). The saddle point contributions are

$$\text{Branch 2A :} \quad 1 \quad \text{for any value of } \beta \quad (3.15)$$

$$\text{Branch 2B :} \quad \exp[-I^{os,-}(\beta, r_b, \Lambda)] \quad \text{for } \beta \leq \beta_{cr}(r_b, \Lambda) \quad (3.16)$$

$$\text{Branch 2C :} \quad \exp[-I^{os,+}(\beta, r_b, \Lambda)] \quad \text{for } \beta \leq \beta_{cr}(r_b, \Lambda) \quad (3.17)$$

⁶There have been several attempts to derive the E - S relationship beyond the maximum energy $\frac{r_b}{G}$ [13, 15, 16, 17]. Although the detailed behaviors of their entropy functions differ, all their maximum entropies are $\frac{\pi}{G}r_b^2$, which is located at $E = \frac{r_b}{G}$.

where the on-shell action functions $I^{os,-}$ and $I^{os,+}$ are given by

$$I^{os,\pm}(\beta, r_b, \Lambda) \equiv \frac{-1}{G} \left[\frac{4\pi}{1 - \Lambda r_H^\pm(\beta, r_b, \Lambda)^2} \left\{ r_H^\pm(\beta, r_b, \Lambda) \left(r_b - \frac{\Lambda}{3} r_b^3 \right) - \frac{3}{4} r_H^\pm(\beta, r_b, \Lambda)^2 + \frac{\Lambda}{12} r_H^\pm(\beta, r_b, \Lambda)^4 \right\} - r_b \beta \sqrt{1 - \frac{\Lambda}{3} r_b^2} \right] \quad (3.18)$$

and r_H^- and r_H^+ are the positive roots of

$$\frac{16\pi^2\Lambda}{3r_b} r_H^5 - \Lambda^2 \beta^2 r_H^4 - \frac{16\pi^2}{r_b} r_H^3 + \left(16\pi^2 - \frac{16\pi^2\Lambda r_b^2}{3} + 2\Lambda\beta^2 \right) r_H^2 - \beta^2 = 0 \quad (3.19)$$

for $\beta < \beta_{cr}(r_b, \Lambda)$. r_H^- is the smaller one and r_H^+ is the larger one. β_{cr} is defined by

$$\beta_{cr}(r_b, \Lambda) = \frac{4\pi r_{H,cr}(r_b, \Lambda)}{1 - \Lambda r_{H,cr}(r_b, \Lambda)^2} \sqrt{\left(1 - \frac{\Lambda}{3} r_b^2 \right) - \frac{r_{H,cr}(r_b, \Lambda)}{r_b} + \frac{\Lambda}{3r_b} r_{H,cr}(r_b, \Lambda)^3} \quad (3.20)$$

and $r_{H,cr}$ is the positive root of

$$-\frac{\Lambda^2}{6r_b} r_H^5 + \frac{\Lambda}{3r_b} r_H^3 + \Lambda \left(1 - \frac{\Lambda}{3} r_b^2 \right) r_H^2 - \frac{3}{2r_b} r_H + \left(1 - \frac{\Lambda}{3} r_b^2 \right) = 0 \quad (3.21)$$

The transition inverse temperature is given by

$$\beta_{tr}(r_b, \Lambda) = \frac{4\pi r_{H,tr}(r_b, \Lambda)}{1 - \Lambda r_{H,tr}(r_b, \Lambda)^2} \sqrt{\left(1 - \frac{\Lambda}{3} r_b^2 \right) - \frac{r_{H,tr}(r_b, \Lambda)}{r_b} + \frac{\Lambda}{3r_b} r_{H,tr}(r_b, \Lambda)^3} \quad (3.22)$$

and $r_{H,tr}$ is the positive root of

$$\frac{\Lambda^2}{144} r_H^6 - \frac{\Lambda}{8} r_H^4 - \frac{\Lambda}{6} \left(1 - \frac{\Lambda}{3} r_b^2 \right) r_b r_H^3 + \frac{9}{16} r_H^2 - \frac{1}{2} \left(1 - \frac{\Lambda}{3} r_b^2 \right) r_b r_H = 0 \quad (3.23)$$

For general values of $\Lambda < 0$, we cannot obtain exact expressions for β_{cr} , β_{tr} , and so on, contrary to the case of $\Lambda = 0$. We could know them, however, for large $|\Lambda|$. For example,

$$r_{H,cr}(r_b, \Lambda) \simeq \frac{1}{\sqrt{-\Lambda}} \quad \text{for } |\Lambda| \gg 1 \quad (3.24)$$

$$r_{H,tr}(r_b, \Lambda) \simeq \sqrt{\frac{3}{-\Lambda}} \quad \text{for } |\Lambda| \gg 1 \quad (3.25)$$

and correspondingly,

$$\beta_{cr} \rightarrow \frac{2\pi}{\sqrt{3}} r_b \quad (\Lambda \rightarrow -\infty) \quad (3.26)$$

$$\beta_{tr} \rightarrow \pi r_b \quad (\Lambda \rightarrow -\infty) \quad (3.27)$$

The qualitative behavior of free energies and the behaviors of the critical and transition points are shown in Fig. 3. The behavior is qualitatively the same as that in the $\Lambda = 0$ case; branch 2A is

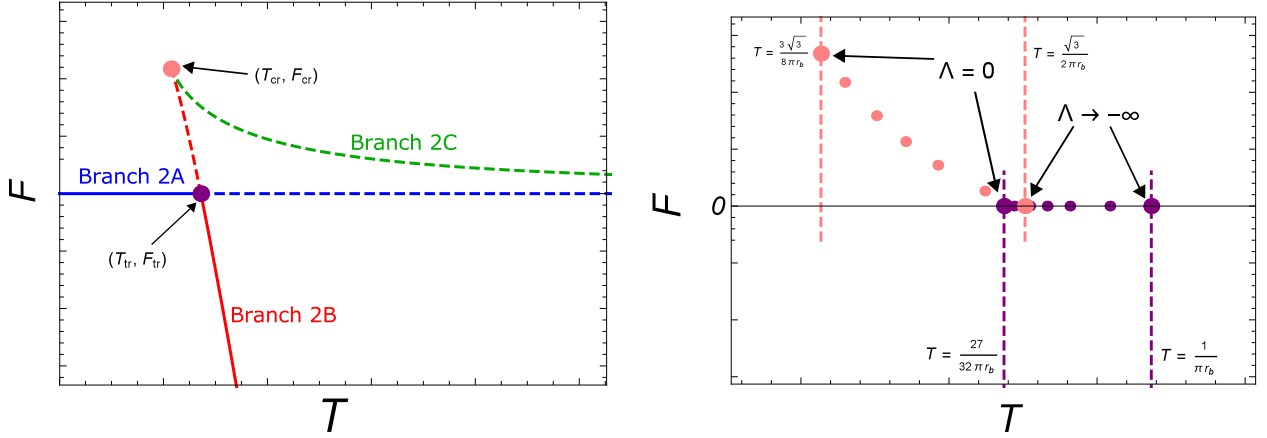


Figure 3: **(Left)** Qualitative behavior of free energies of saddles 2A, 2B, and 2C. The portion that does not give a dominant contribution is dashed. The critical point and the transition point are marked. The temperature and free energy at those points are $T_{cr(tr)} = 1/\beta_{cr(tr)}(r_b, \Lambda)$ and $F_{cr(tr)} = I^{os,+}(\beta_{cr(tr)}, r_b, \Lambda)/\beta_{cr(tr)}(r_b, \Lambda) = I^{os,-}(\beta_{cr(tr)}, r_b, \Lambda)/\beta_{cr(tr)}(r_b, \Lambda)$. **(Right)** Behaviors of critical point and transition point against Λ on T - F plane.

dominant when $T \in [0, 1/\beta_{tr}(r_b, \Lambda)]$, branch 2B is when $T \in [1/\beta_{tr}(r_b, \Lambda), \infty]$, and branch 2C is never dominant. The behaviors of the critical point and the transition point on the T - F plane are also shown in Fig. 3. The Λ dependence of β_{cr} and β_{tr} is weak and they are inversely proportional to r_b , i.e. , $1/\beta_{cr}(r_b, \Lambda) \in \left[\frac{3\sqrt{3}}{8\pi r_b}, \frac{\sqrt{3}}{2\pi r_b}\right]$ and $1/\beta_{tr}(r_b, \Lambda) \in \left[\frac{27}{32\pi r_b}, \frac{1}{\pi r_b}\right]$.

The behavior of entropy against energy is shown in Fig. 4. This is also qualitatively the same as in the previous case. The maximum entropy does not depend on Λ . Therefore, the entropy bound may be given by the area of the boundary over $4G$, independent of $\Lambda \leq 0$. On the other hand, the maximum energy is highly dependent on Λ and goes to infinity as we increase $|\Lambda|$. The energy and entropy at the critical point are given by

$$E_{cr}(r_b, \Lambda) = \frac{r_b}{G} \left[\sqrt{1 - \frac{\Lambda}{3} r_b^2} - \sqrt{\left(1 - \frac{\Lambda}{3} r_b^2\right) - \frac{r_{H,cr}(r_b, \Lambda)}{r_b} + \frac{\Lambda}{3r_b} r_{H,cr}(r_b, \Lambda)^3} \right] \quad (3.28)$$

$$S_{cr}(r_b, \Lambda) = \frac{\pi}{G} r_{H,cr}(r_b, \Lambda)^2 \quad (3.29)$$

The behaviors of the critical point and the maximum entropy point are also shown in Fig. 4. As I mentioned above, the maximum energy goes to infinity, with fixing the maximum entropy, as we increase $|\Lambda|$. On the other hand, the critical point goes to $(0,0)$. Therefore, the ratio of the thermodynamically stable energy range $\left[E_{cr}(r_b, \Lambda), \frac{r_b}{G} \sqrt{1 - \frac{\Lambda}{3} r_b^2} \right]$ to the whole energy range $\left[0, \frac{r_b}{G} \sqrt{1 - \frac{\Lambda}{3} r_b^2} \right]$ increases.

We have seen the thermodynamical properties for the $\Lambda \leq 0$ case. Some are universal, irrelevant of the precise value of Λ , and others are highly dependent on it. Let me summarize them here:

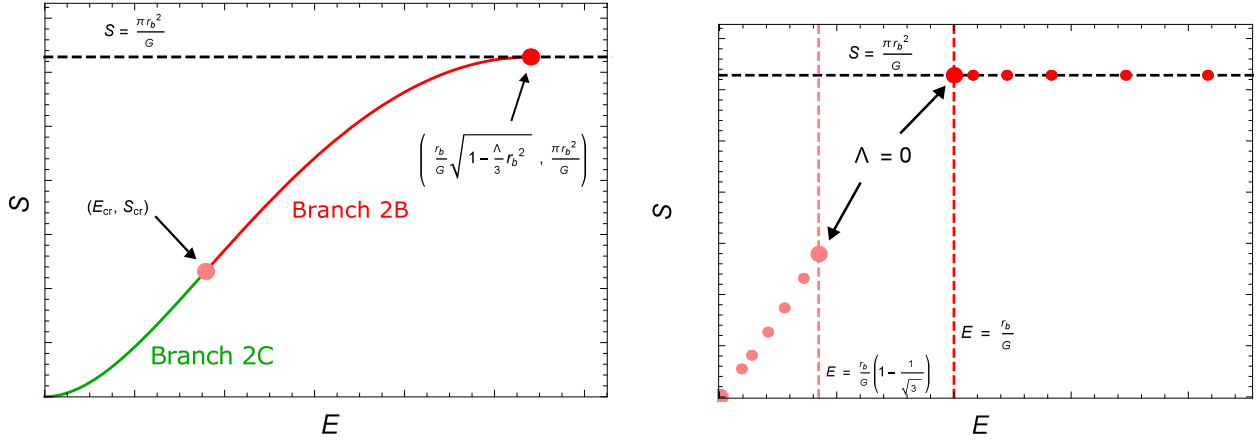


Figure 4: **(Left)** Qualitative behavior of entropy as a function of energy. The critical point and the maximum entropy point are marked. The energy and entropy at the critical point are given by $E_{cr} = E_{cr}(r_b, \Lambda)$ and $S_{cr} = \frac{\pi r_{H,cr}(r_b, \Lambda)^2}{G}$ (see the main text). The maximal energy and entropy are $\frac{r_b}{G} \sqrt{1 - \frac{\Lambda}{3} r_b^2}$ and $\frac{\pi r_b^2}{G}$. **(Right)** Behaviors of critical point and maximum entropy point against Λ on E - S plane.

- Universal
 - Thermodynamically stable.
 - There exist two phases: radiation and BH.
 - The transition temperature and the critical temperature are always given by $\frac{a(\Lambda, r_b)}{r_b}$, where $0.206 < a(\Lambda, r_b) < 0.319$.
 - The maximum entropy is given by $\frac{\pi r_b^2}{G}$.
 - Λ dependent
 - The maximum energy goes to infinity as $|\Lambda|$ is increased.
 - The critical energy (and the critical entropy) decreases as $|\Lambda|$ is increased.
- Consequently, the ratio of the thermodynamically stable region increases and goes to 1 when $\Lambda \rightarrow -\infty$.

3.3 $\Lambda > 0$

Contrary to the $\Lambda < 0$ case, there are few studies of the $\Lambda > 0$ case. (From different perspectives, “thermodynamics of de Sitter space” or “thermodynamics of de Sitter BH” is investigated in the literature, for instance, [24, 23, 25, 26, 27, 28].) I restrict the analysis to $0 < \Lambda < \frac{3}{r_b^2}$. At the end of this subsection, I will give very brief comments on the $\frac{3}{r_b^2} \leq \Lambda$ case.

3.3.1 $0 < \Lambda < \frac{3}{r_b^2}$

Firstly, there exist similar saddle points to those in the $\Lambda \leq 0$ case:

$$\mathbf{g}(x) = f(r)d\tau^2 + \frac{1}{f(r)}dr^2 + r^2(d\theta^2 + \sin^2\theta d\phi^2) \quad (3.30)$$

$$f(r) = 1 - \frac{\Lambda}{3}r^2 \quad \text{for } B^3 \times S^1 \text{ topology} \quad (3.31)$$

$$f(r) = 1 - \frac{2Gm}{r} - \frac{\Lambda}{3}r^2 \quad \text{for } S^2 \times D \text{ topology} \quad (3.32)$$

where the coordinate ranges of r and τ , $[r_H, r_b]$ and $[0, \beta_0]$, and the mass parameter m satisfy the following conditions (see Fig. 1):

$$f(r_H) = 0, \quad \frac{4\pi}{f'(r_H)} = \beta_0, \quad \sqrt{f(r_b)}\beta_0 = \beta, \quad 4\pi r_b^2 = A \quad \text{for } S^2 \times D \text{ topology} \quad (3.33)$$

$$r_H = 0, \quad \sqrt{f(r_b)}\beta_0 = \beta, \quad 4\pi r_b^2 = A \quad \text{for } B^3 \times S^1 \text{ topology} \quad (3.34)$$

Additionally, there also exists the following saddle point in the $S^2 \times D$ topology sector:

$$\mathbf{g}(x) = f(r)d\tau^2 + \frac{1}{f(r)}dr^2 + r^2(d\theta^2 + \sin^2\theta d\phi^2) \quad (3.35)$$

$$f(r) = 1 - \frac{2Gm}{r} - \frac{\Lambda}{3}r^2 \quad (3.36)$$

$$\text{coordinate : } \tau \in [0, \beta_0], \quad r \in [r_b, r_c] \quad (3.37)$$

$$\text{condition : } f(r_c) = 0, \quad \frac{4\pi}{f'(r_c)} = -\beta_0, \quad \sqrt{f(r_b)}\beta_0 = \beta, \quad 4\pi r_b^2 = A \quad (3.38)$$

The difference from Eq. (3.32) is that the boundary is now located at the smaller end of r and the bolt [29] is at the larger end $r = r_c$.⁷ Since the position of the bolt is at the larger end of the r coordinate, we have a minus sign in the smoothness condition there (Fig. 5). For fixed r_b , r_c can be arbitrarily large depending on β . This is in contrast to the saddle point (3.32) (and (3.12) or (3.2) in the case of $\Lambda \leq 0$), whose entropy, that is, the area of the bolt, is always bounded by $4\pi r_b^2$. Since this saddle point enables the system to contain arbitrarily large entropy, as we will see shortly, I call such a Euclidean geometry, of which the area of the bolt is greater than the area of the boundary, the ‘‘bag of gold (BG) instanton,’’ after Wheeler’s bag of gold spacetime.^{8 9} Eventually, except for the special case that I will explain shortly, the saddle point contributions are

$$\text{Branch 3A : } \quad 1 \quad \text{for any value of } \beta \quad (3.39)$$

$$\text{Branch 3B : } \quad \exp[-I^{os,-}(\beta, r_b, \Lambda)] \quad \text{for } \beta \leq \beta_{cr}(r_b, \Lambda) \quad (3.40)$$

$$\text{Branch 3C : } \quad \exp[-I^{os,+}(\beta, r_b, \Lambda)] \quad \text{for } \beta \leq \beta_{cr}(r_b, \Lambda) \quad (3.41)$$

$$\text{Branch 3D : } \quad \exp[-I^{os,BG}(\beta, r_b, \Lambda)] \quad \text{for any value of } \beta \quad (3.42)$$

⁷The reason why I use ‘‘c’’ is because it is the Euclidean counterpart of the cosmological horizon.

⁸Wheeler’s bag of gold spacetime can contain an arbitrary amount of entropy in space. The BG instanton can contain an arbitrary amount of ‘‘entropy’’ in the ‘‘Euclidean holographic plate.’’ (However, attention must be paid to the former statement because it may not be true when the matter couples to the dynamical gravity [30].)

⁹Note that the solution itself is not new or surprising. I do not know who first introduced this kind of solution into physics. For example, in [31], they presented the Lorentzian (and topologically generalized) version of (3.35) (when $m < 0$) without the boundary $r = r_b$ but with a singularity at the center $r = 0$. They called it ‘‘topological de Sitter.’’

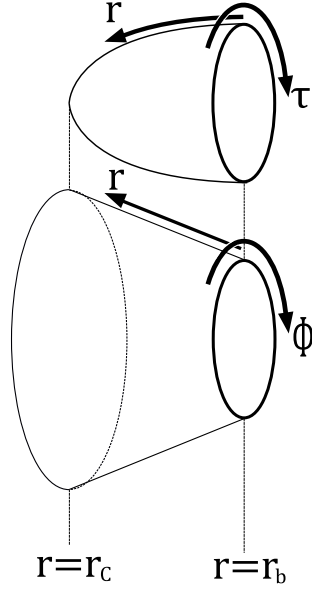


Figure 5: Extra saddle point geometry of $S^2 \times D$ topology (BG instanton). The area of the bolt $4\pi r_c^2$ is larger than that of the boundary $4\pi r_b^2$. For fixed r_b , r_c can be arbitrarily large depending on β . Branch 3D consists of this type of geometry.

The definition of $I^{os,+}$, $I^{os,-}$ is the same as (3.18), and that of $I^{os,BG}$ is (3.18) with r_H^\pm replaced by r_c :

$$I^{os,BG}(\beta, r_b, \Lambda) \equiv \frac{-1}{G} \left[\frac{4\pi}{1 - \Lambda r_c(\beta, r_b, \Lambda)^2} \left\{ r_c(\beta, r_b, \Lambda) \left(r_b - \frac{\Lambda}{3} r_b^3 \right) - \frac{3}{4} r_c(\beta, r_b, \Lambda)^2 + \frac{\Lambda}{12} r_c(\beta, r_b, \Lambda)^4 \right\} - r_b \beta \sqrt{1 - \frac{\Lambda}{3} r_b^2} \right] \quad (3.43)$$

r_c , r_H^+ , and r_H^- in (3.43) and (3.18) are defined as the largest, the middle, and the smallest of the positive roots of Eq. (3.19) for $\beta < \beta_{cr}(r_b, \beta)$, and for $\beta > \beta_{cr}(r_b, \beta)$, r_c is the positive root of the equation. The definition of β_{cr} is the same as before. When $\Lambda = \frac{1}{r_b^2}$, branch 3B ceases to exist and the behaviors of branches 3C and 3D change: ¹⁰

$$\text{Branch 3A :} \quad 1 \quad \text{for any value of } \beta \quad (3.44)$$

$$\text{Branch 3C :} \quad \exp[-I^{os,-}(\beta, r_b, \Lambda)] \quad \text{for } \beta \leq \frac{2\pi}{\sqrt{\Lambda}} \quad (3.45)$$

$$\text{Branch 3D :} \quad \exp[-I^{os,BG}(\beta, r_b, \Lambda)] \quad \text{for } \beta > \frac{2\pi}{\sqrt{\Lambda}} \quad (3.46)$$

¹⁰When Λ takes this value (or, when we put the boundary $r = r_b$ appropriately for a given Λ), both the $r_H \rightarrow r_b$ limit of Euclidean BH and the $r_c \rightarrow r_b$ limit of BG instanton corresponds to the Nariai limit, that is, the resulting geometry is half of Euclidean Nariai geometry in the static patch. Therefore, two branches 3C and 3D are smoothly connected and their thermodynamical quantities do not diverge unlike the $\Lambda \neq \frac{1}{r_b^2}$ case.

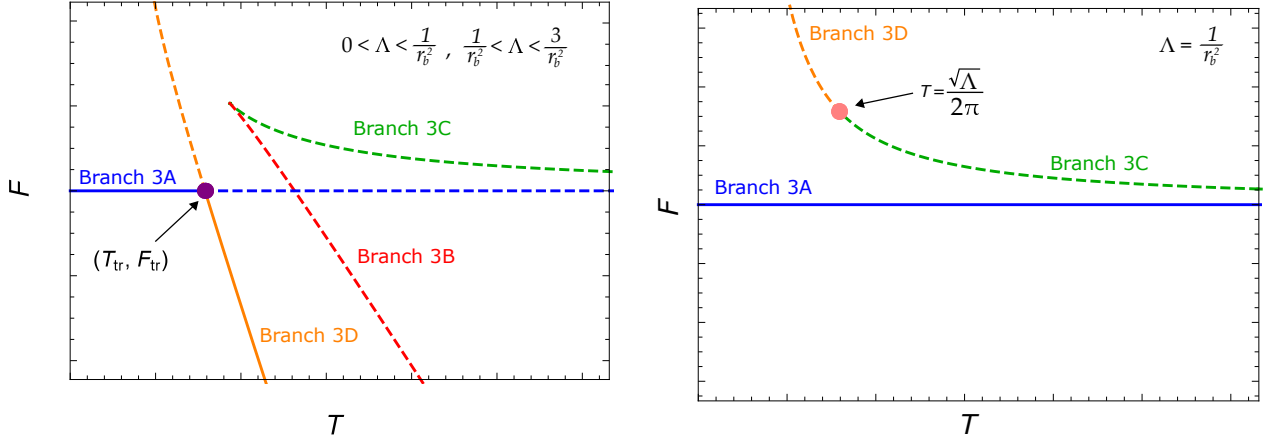


Figure 6: Qualitative behaviors of free energies for $0 < \Lambda < \frac{3}{r_b^2}$ case. **(Left)** $\Lambda \neq \frac{1}{r_b^2}$ case. Below T_{tr} , branch 3A dominates; above T_{tr} , branch 3D dominates. **(Right)** $\Lambda = \frac{1}{r_b^2}$ case. Branch 3A always dominates and there exist (thermodynamically unstable) subdominant branches for all T . This structure is similar to that of asymptotically flat spacetime.

The qualitative behaviors of free energies for each case are shown in Fig. 6. For the $\Lambda \neq \frac{1}{r_b^2}$ case, although the behaviors of 3A, 3B, and 3C are qualitatively the same as before, the dominant saddle at high temperature becomes 3D, that is, the BG instanton. For the $\Lambda = \frac{1}{r_b^2}$ case, branches 3C and 3D become subdominant for all T and 3A is always dominant.

I also show the corresponding entropy behaviors against energy in Fig. 7. For $0 < \Lambda < \frac{1}{r_b^2}$, the entropy bound $S = \frac{\pi r_b^2}{G}$ is attained by the rightmost of 3B. This is exactly the same as the $\Lambda \leq 0$ case, where the energy and entropy at the rightmost of branch 2B are given by $\left(\frac{r_b}{G} \sqrt{1 - \frac{\Lambda}{3} r_b^2}, \frac{\pi r_b^2}{G}\right)$. The difference is the existence of branch 3D and it starts from the point $\left(\frac{r_b}{G} \sqrt{1 - \frac{\Lambda}{3} r_b^2}, \frac{\pi r_b^2}{4G} \left(\sqrt{\frac{12}{\Lambda r_b^2} - 3} - 1\right)^2\right)$. The entropy difference between the rightmost of 3B and the leftmost of 3D becomes small as we increase Λ , and finally becomes zero at $\Lambda = \frac{1}{r_b^2}$. Above that value, the leftmost of 3D is fixed to the maximum entropy line and the rightmost of 3B detaches and starts to decrease. They go to $\left(0, \frac{\pi r_b^2}{G}\right)$ and $(0, 0)$ respectively as we increase Λ to $\frac{3}{r_b^2}$.

In previous subsections, we have seen that *thermodynamical stability* and *the entropy bound* are universal properties for $\Lambda \leq 0$. I will argue that both are absent for $\Lambda > 0$.

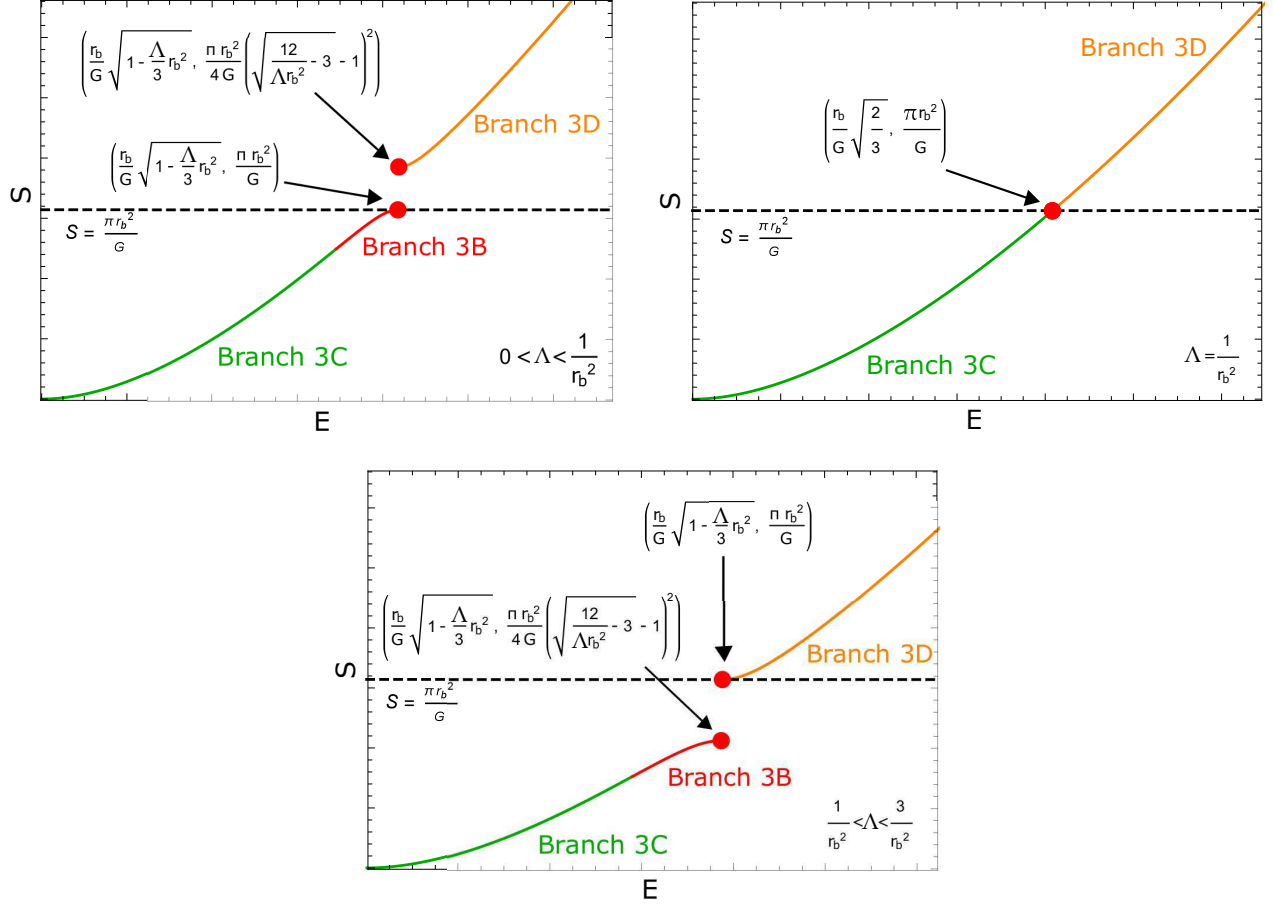


Figure 7: Qualitative behaviors of entropy for $0 < \Lambda < \frac{3}{r_b^2}$ case. The dashed lines represent the entropy bound $S = \frac{\pi r_b^2}{G}$. **(Left)** $0 < \Lambda < \frac{1}{r_b^2}$ case. The rightmost of 3B is at $\left(\frac{r_b}{G} \sqrt{1 - \frac{\Lambda}{3} r_b^2}, \frac{\pi r_b^2}{G}\right)$, the leftmost of 3D is at $\left(\frac{r_b}{G} \sqrt{1 - \frac{\Lambda}{3} r_b^2}, \frac{\pi r_b^2}{4G} \left(\sqrt{\frac{12}{\Lambda r_b^2} - 3} - 1\right)^2\right)$. **(Right)** $\Lambda = \frac{1}{r_b^2}$ case. For only this value of Λ , the endpoints of the two branches meet on the entropy bound line. **(Bottom)** $\frac{1}{r_b^2} < \Lambda < \frac{3}{r_b^2}$ case. The leftmost of 3D attaches to the line at $\left(\frac{r_b}{G} \sqrt{1 - \frac{\Lambda}{3} r_b^2}, \frac{\pi r_b^2}{G}\right)$ and the rightmost of 3B detaches from the line and is located at $\left(\frac{r_b}{G} \sqrt{1 - \frac{\Lambda}{3} r_b^2}, \frac{\pi r_b^2}{4G} \left(\sqrt{\frac{12}{\Lambda r_b^2} - 3} - 1\right)^2\right)$.

Absence of thermodynamical stability

Firstly, let us see properties of branch 3D for the $\Lambda \neq \frac{1}{r_b^2}$ case. Since $\frac{\partial E}{\partial T} < 0$ always holds on branch 3D,¹¹ it is thermodynamically unstable. This means that, above T_{tr} , the system does not settle down to thermal equilibrium. One might think, then, that thermal equilibrium would be realized below T_{tr} as thermal dS spacetime. But that is not the case. Even if the thermal dS spacetime seems to be stable, it may transition to the BG spacetime¹² with a small probability $\sim e^{-I^{os,BG}}$. Because, as stated above, it is thermodynamically unstable, it can induce eternal growth of the cosmological horizon and will not maintain equilibrium any longer. Therefore, even if the thermodynamically stable branch 3A dominates below T_{tr} , the system cannot be thermodynamically stable owing to the instanton effect. This is essentially the same reasoning by which the authors concluded that *hot flat space is unstable* in [32]. Applying the latter discussion to the $\Lambda = \frac{1}{r_b^2}$ case, we can also conclude that the system is thermodynamically unstable for that case.

Generally, if there exists a thermodynamically unstable saddle, the endpoints of its branch must be bounded by thermodynamically stable branches in order for the system to be thermodynamically stable, for example, as is branch 2C in Fig. 3.

Absence of the entropy bound

Since I argued that the system is thermodynamically unstable, we may not be able to regard Fig. 7 as an $E-S$ relation in thermal equilibrium. Instead, we should view it as the relation of equilibrium states of isolated setting or the density of states of the system. From that point of view, the relation Fig. 7 tells us the system can contain arbitrary entropy, or the density of states indefinitely grows as we increase the energy. In this sense, the system does not have the entropy bound.

3.3.2 $\frac{3}{r_b^2} \leq \Lambda$

Above $\Lambda = \frac{3}{r_b^2}$, branches 3A, 3B, and 3C cease to exist. The only remaining Euclidean saddle is 3D. Owing to the choice of the subtraction term (2.3), the energy of the branch becomes complex. I do not know how to interpret or remedy this. Additionally, I do not know whether we should include the contribution from the saddle 3D because Euclidean path integrals of general relativity may ultimately be defined by some purely complex integration contour [22], as I will comment in the final section. I hope these points will be clarified in the future work [33].

4 Gravitoscalar thermodynamics with a simple potential

Assuming all the Euclidean saddle points contribute to the partition function, I have shown that the properties of the system drastically change depending on Λ . The next thing I want to do is to add

¹¹Branch 3D is parameterized by the radius of the cosmological horizon $r_c \in \left[\max \left(r_b, \frac{r_b}{2} \left(\sqrt{\frac{12}{\Lambda r_b^2} - 3} - 1 \right) \right), \infty \right)$ for given r_b and Λ . We can easily show that $E_{3D}(r_c) = \frac{r_b}{G} \left[\sqrt{1 - \frac{\Lambda}{3} r_b^2} - \sqrt{\left(1 - \frac{\Lambda}{3} r_b^2\right) - \frac{r_c}{r_b} + \frac{\Lambda}{3 r_b} r_c^3} \right]$ and $\beta_{3D}(r_c) = -\frac{4\pi r_c}{1 - \Lambda r_c^2} \sqrt{\left(1 - \frac{\Lambda}{3} r_b^2\right) - \frac{r_c}{r_b} + \frac{\Lambda}{3 r_b} r_c^3}$ are monotonically increasing functions in that range.

¹²This is *not* Wheeler's bag of gold spacetime but the Lorentzian continuation of the BG instanton.

a new entity into the system and investigate its properties, especially focusing on thermodynamical stability and the existence of the entropy bound. In this paper, as a simple extension, I consider a gravity-scalar system with φ^2 potential (2.9). In addition to the parameter M , the mass of the scalar field, we have the external field $J_\varphi(y) \equiv \varphi(y)$ ($y \in \partial\mathcal{M}$) for parameterizing the theory.^{13 14} In order to realize thermal equilibrium in the Lorentzian theory, I take J_φ to be constant over (boundary) space and time. Correspondingly, it is also for the Euclidean boundary. I mainly focus on the J_φ dependence of thermodynamical properties rather than M because non-zero J_φ will generally induce non-trivial scalar field configurations on the saddle point geometries. I will discuss qualitatively the conditions for the existence of saddle point geometries in subsection 4.1 and the behaviors of thermodynamic potentials in subsection 4.2.

4.1 Conditions for the existence of saddle points

As we saw in subsection 3.3, the horizon radius r_H of a Euclidean BH is in the range $(0, r_b)$ when $0 < \Lambda \leq \frac{1}{r_b^2}$, in $(0, \frac{r_b}{2} \sqrt{\frac{12}{\Lambda r_b^2} - 3} - 1)$ when $\frac{1}{r_b^2} < \Lambda \leq \frac{3}{r_b^2}$, and Euclidean BHs cease to exist when $\Lambda > \frac{3}{r_b^2}$ in the pure gravity system. On the other hand, the range of the horizon radius of the BG instanton is $(\frac{r_b}{2} \sqrt{\frac{12}{\Lambda r_b^2} - 3} - 1, \infty)$ when $0 < \Lambda \leq \frac{1}{r_b^2}$ and (r_b, ∞) when $\frac{1}{r_b^2} < \Lambda$. I would like to discuss similar conditions on J_φ in this system.

The types of saddle point geometry are essentially the same as before, but generally with a scalar cloud. The forms of metric and scalar are as follows:

$$\begin{aligned} \mathbf{g}(x) &= f(r)e^{-2\delta(r)}d\tau^2 + \frac{1}{f(r)}dr^2 + r^2(d\theta^2 + \sin^2\theta d\phi^2) \\ \varphi(x) &= \varphi(r) \end{aligned} \quad (4.2)$$

where the coordinate ranges of r and τ , $[r_H, r_b]$ and $[0, \beta_0]$, and the functions f , δ , and φ must satisfy the following conditions:

$$f(r_H) = 0, \quad \frac{4\pi}{f'(r_H)}e^{\delta(r_H)} = \beta_0, \quad \varphi'(r_H) = \frac{M^2\varphi(r_H)}{f'(r_H)}, \quad \text{for } S^2 \times D \text{ topology} \quad (4.3)$$

$$\sqrt{f(r_b)}e^{-\delta(r_b)}\beta_0 = \beta, \quad 4\pi r_b^2 = A, \quad \varphi(r_b) = J_\varphi$$

$$r_H = 0, \quad f(0) = 1, \quad \varphi'(0) = 0,$$

$$\sqrt{f(r_b)}e^{-\delta(r_b)}\beta_0 = \beta, \quad 4\pi r_b^2 = A, \quad \varphi(r_b) = J_\varphi \quad \text{for } B^3 \times S^1 \text{ topology} \quad (4.4)$$

¹³ $J_\varphi(y)$ is, of course, just a boundary condition in terms of the gravitational theory. However, it is an external field in terms of the holographic field theory.

¹⁴Although, together with the operator

$$\mathcal{O}_\varphi \equiv \int_{S^2} d^2z \sqrt{\sigma} n_\nu \nabla^\nu \varphi, \quad (4.1)$$

$(J_\varphi, \mathcal{O}_\varphi)$ form conjugate variables on the boundary, they cannot be regarded as thermodynamical variables, unlike the boundary conjugate pair of the $U(1)$ gauge field. This is because \mathcal{O}_φ is not a conserved charge. In essentially the same sense, I do not regard the cosmological constant and thermodynamical volume [34, 35, 26] as thermodynamical variables in this paper. (See also footnote 3.)

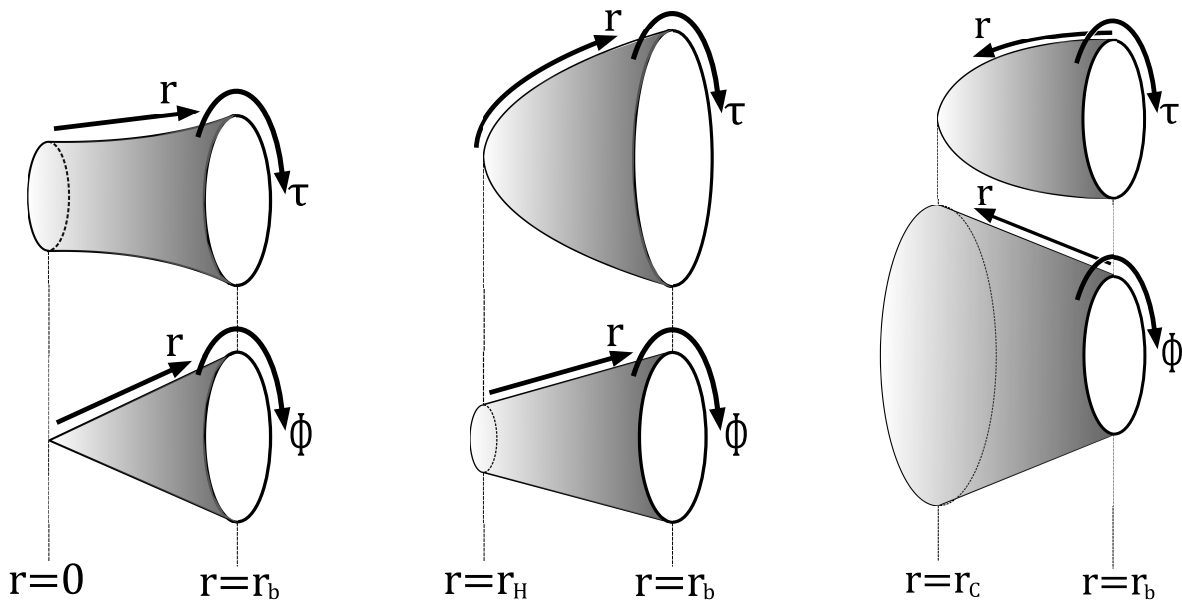


Figure 8: Types of saddle point. Their geometries are qualitatively similar to those of the pure gravity case. The gradation schematically represents the value of the scalar field. **(Left)** Euclidean soliton ($B^3 \times S^1$ topology). **(Middle)** Euclidean BH ($S^2 \times D$ topology). **(Right)** BG instanton ($S^2 \times D$ topology).

Since the latter is the Euclidean version of solitonic solutions, I call it a Euclidean soliton. For some case, the BG instanton may exist. In that case, the coordinate range of r is $[r_b, r_c]$ and the variables must satisfy the following:

$$\begin{aligned}
 f(r_c) = 0, \quad \frac{4\pi}{f'(r_c)} e^{\delta(r_c)} = -\beta_0, \quad \varphi'(r_c) = \frac{M^2 \varphi(r_c)}{f'(r_c)}, & \quad \text{for } S^2 \times D \text{ topology} \\
 \sqrt{f(r_b)} e^{-\delta(r_b)} \beta_0 = \beta, \quad 4\pi r_b^2 = A, \quad \varphi(r_b) = J_\varphi & \quad \text{(BG instanton)} \quad (4.5)
 \end{aligned}$$

These saddles are shown schematically in Fig. 8.

The radius of S^2 of all solutions described above is monotonically increasing or decreasing. This behavior is the same as that for pure gravity with $\Lambda > 0$. However, in this gravity-scalar system, there exist other types of solutions, of which the radius of S^2 firstly increases and then decreases (Fig. 9). I call these types of solutions ‘‘Euclidean PL-soliton,’’ ‘‘Euclidean PL-BH,’’ and ‘‘PL-BG instanton,’’ respectively.¹⁵

All the solutions described above will be obtained by integrating the equation of motion numerically. The details and some examples of numerical solutions are given in Appendix A. In addition, rigorously speaking, PL solutions cannot be described by the form of the metric (4.2); that is, we have to use other coordinates and choices of metric functions. These details will also be explained in Appendix A.

¹⁵PL denotes ‘‘Python’s Lunch’’ [36], *only* due to its shape.

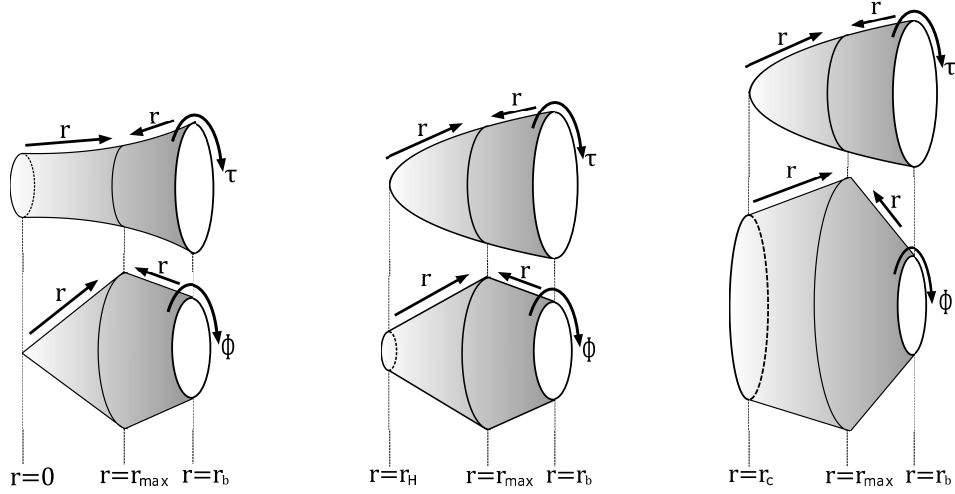


Figure 9: Three types of PL geometry whose S^2 radius grows from the boundary, reaches some maximum radius r_{max} , and shrinks toward the center or the bolt. The gradation schematically represents the value of the scalar field. **(Left)** Euclidean PL-soliton ($B^3 \times S^1$ topology). **(Middle)** Euclidean PL-BH ($S^2 \times D$ topology). **(Right)** PL-BG instanton ($S^2 \times D$ topology).

Below, I will classify the structure of the existence of solutions on $J_\varphi - r_{H(c)}$ plane by the value of Λ . For some cases, however, it highly depends on r_b and M so that it is difficult to show its qualitative properties exhaustively. For these cases, I just give some examples of the structure and I mark these cases with (*).

Euclidean BH and Euclidean soliton

Similar to the $\Lambda > 0$ case, J_φ does not affect the existence of Euclidean BHs if it is sufficiently small but does if it is not. I define $r_{H,max}(r_b, \Lambda, J_\varphi, M)$ as the maximum horizon radius for given parameters. The behavior of $r_{H,max}(r_b, \Lambda, J_\varphi, M)$ against J_φ for fixed r_b, Λ, M may be classified into three cases depending on Λ :

- $-\infty < \Lambda < \frac{1}{r_b^2}$

$r_{H,max} = r_b$ for $0 \leq J_\varphi < \sqrt{\frac{1-\Lambda r_b^2}{4\pi G}} \frac{1}{r_b M}$ and it monotonically decreases until reaching some critical value $J_{\varphi, BHcri}(r_b, \Lambda, M)$ where $r_{H,max}(r_b, \Lambda, J_{\varphi, BHcri}(r_b, \Lambda, M), M) = 0$. $r_{H,max} = 0$ for $J_{\varphi, BHcri}(r_b, \Lambda, M) \leq J_\varphi$.¹⁶

- $\frac{1}{r_b^2} < \Lambda < \frac{3}{r_b^2}$

¹⁶For $-\infty < \Lambda < 0$ and $0 < J_\varphi < \sqrt{\frac{-\Lambda}{4\pi G M^2}}$, there always exist solutions for arbitrary $r_b > 0$. One might guess there also exist hairy solutions for asymptotically AdS ($r_b \rightarrow \infty$) case. However, since the energy of these solutions diverges as we increase r_b , the limiting solutions are not physical, or do not contribute to the partition function. This is also true for other types of solution.

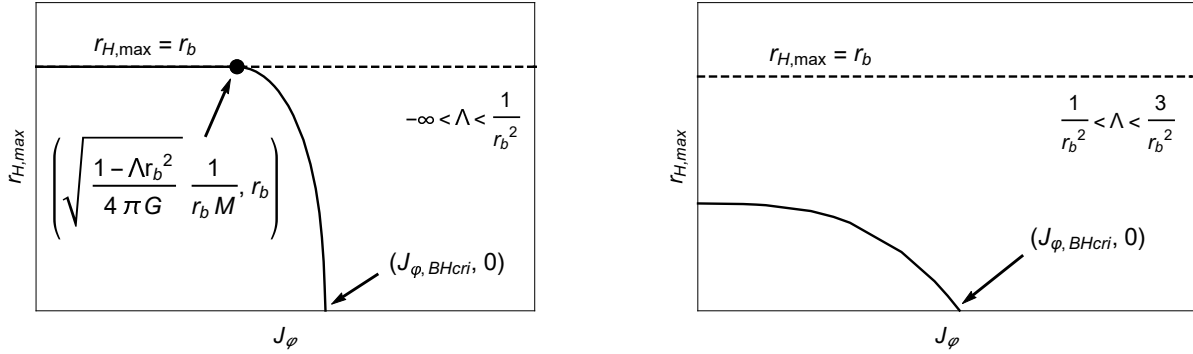


Figure 10: Qualitative behaviors of $r_{H,max}(r_b, \Lambda, J_\varphi, M)$ against J_φ . **(Left)** $-\infty < \Lambda < \frac{1}{r_b^2}$ case. **(Right)** $\frac{1}{r_b^2} < \Lambda < \frac{3}{r_b^2}$ case. As we increase Λ , the curve shrinks and collapses to the point $(0, 0)$ when $\Lambda = \frac{3}{r_b^2}$.

For $0 \leq J_\varphi < J_{\varphi, BHcri}(r_b, \Lambda, M)$, $r_{H,max}$ monotonically decreases from $r_{H,max}(r_b, \Lambda, 0, M) = \frac{r_b}{2} \left(\sqrt{\frac{12}{\Lambda r_b^2} - 3} - 1 \right)$. $r_{H,max} = 0$ for $J_{\varphi, BHcri}(r_b, \Lambda, M) \leq J_\varphi$.

- $\frac{3}{r_b^2} < \Lambda < \infty$

$r_{H,max} = 0$, that is, Euclidean BHs and Euclidean solitons do not exist for any J_φ .

The qualitative behaviors of $r_{H,max}(r_b, \Lambda, J_\varphi, M)$ against J_φ for the first and second cases are shown in Fig. 10.

BG instanton

The range of possible size of the cosmological horizon r_c of the BG instanton depends on not only J_φ but also r_b, Λ, M . The behavior of the range against J_φ for fixed r_b, Λ, M may be roughly classified into three cases depending on Λ :

- $-\infty < \Lambda \leq 0$

There are no BG instantons for $0 \leq J_\varphi \leq \sqrt{\frac{1-\Lambda r_b^2}{4\pi G}} \frac{1}{r_b M}$. For $\sqrt{\frac{1-\Lambda r_b^2}{4\pi G}} \frac{1}{r_b M} < J_\varphi$, the range is $(r_b, r_{c,max}(r_b, \Lambda, J_\varphi, M))$, where $r_{c,max}(r_b, \Lambda, J_\varphi, M)$ is a monotonically increasing function for J_φ . There also exists some critical radius $r_b < r_{c,cr}(r_b, \Lambda, J_\varphi, M) < r_{c,max}(r_b, \Lambda, J_\varphi, M)$, which is also a monotonically increasing function for J_φ . Between $r_{c,max}$ and $r_{c,cr}$, there exist two different solutions with the same r_c . The qualitative behavior of the range is shown in Fig. 11.

- $0 < \Lambda \leq \frac{1}{r_b^2}$ (*)

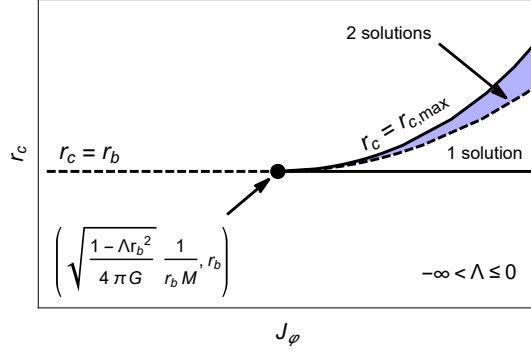


Figure 11: Qualitative behavior of range of possible size of cosmological horizon r_c of BG instanton against J_φ when $-\infty < \Lambda \leq 0$. For $0 \leq J_\varphi \leq \sqrt{\frac{1-\Lambda r_b^2}{4\pi G} \frac{1}{r_b M}}$, there are no BG instantons. Above $\sqrt{\frac{1-\Lambda r_b^2}{4\pi G} \frac{1}{r_b M}}$, there exist BG instantons between $r_{c,max}(r_b, \Lambda, J_\varphi, M)$ and r_b . There exist two solutions with the same r_c in the shaded region.

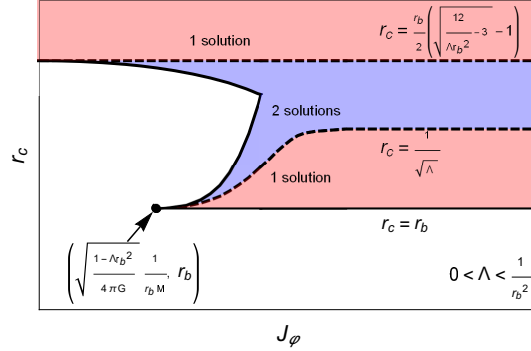


Figure 12: Example of qualitative behavior of range of possible size of cosmological horizon r_c of BG instanton against J_φ when $0 < \Lambda \leq \frac{1}{r_b^2}$. This structure may appear when both Λ/M^2 and $r_b M$ are large enough. This is the simplest structure. If we choose parameters that do not satisfy the above conditions, a more complicated structure will appear, such as Fig. 13. (An example of parameters that exhibit this structure is $(r_b, \Lambda, M) = (5\sqrt{G}, 0.012/G, 0.1/\sqrt{G})$).

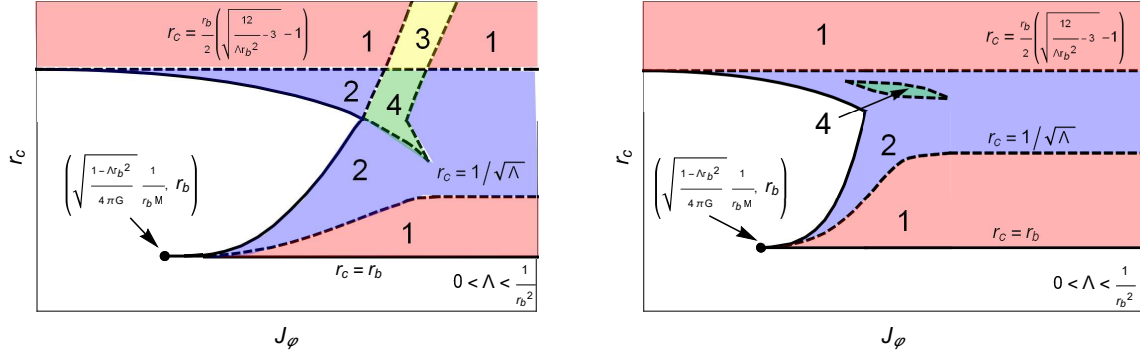


Figure 13: Other examples of qualitative behavior of range of possible size of cosmological horizon r_c of BG instanton against J_φ when $0 < \Lambda \leq \frac{1}{r_b^2}$. The numbers in the figures represent the number of solutions with the same r_c and J_φ . (Examples of parameters that exhibit these structures are $(r_b, \Lambda, M) = (7\sqrt{G}, 0.002/G, 0.1/\sqrt{G})$ (Left) and $(r_b, \Lambda, M) = (3\sqrt{G}, 0.0056/G, 0.1/\sqrt{G})$ (Right).)

Contrary to the above case, there exist BG instantons for all J_φ , and the structure of the existence domain and the number of instanton solutions are complicated and depend on the other parameters r_b and M . The qualitative behaviors that do not depend on r_b and M are as follows:

- for sufficiently small J_φ , the existence range is $[r_{c,min}(r_b, \Lambda, J_\varphi, M), \infty)$, where $r_{c,min}$ is a monotonically decreasing function for J_φ , $r_{c,min}(r_b, \Lambda, 0, M) = \frac{r_b}{2} \left(\sqrt{\frac{12}{\Lambda r_b^2} - 3} - 1 \right)$ and greater than r_b ,
- for sufficiently small J_φ , between $\frac{r_b}{2} \left(\sqrt{\frac{12}{\Lambda r_b^2} - 3} - 1 \right)$ and $r_{c,min}(r_b, \Lambda, J_\varphi, M)$, there exist two different solutions with the same r_c ,
- for $\sqrt{\frac{1-\Lambda r_b^2}{4\pi G}} \frac{1}{r_b M} \leq J_\varphi$, the smallest cosmological horizon is r_b ,
- when J_φ is greater than some critical value, the range of cosmological horizon is $[r_b, \infty)$.

Some examples of the qualitative behaviors of the range are shown in Fig. 12, 13. The simplest structure would be Fig. 12. This may be realized when the ratio Λ/M^2 is sufficiently large and the ratio of the boundary radius r_b to the Compton wavelength $\frac{1}{M}$ is also sufficiently large, that is, when the effect of the scalar field is minimum (but still non-trivial). When one of the conditions ceases to hold, the structure becomes complicated, such as Fig. 13.¹⁷

- $\frac{1}{r_b^2} < \Lambda < \infty$

There exist BG instantons for all J_φ . The range is $[r_b, \infty)$ and the number of solutions is one.

¹⁷This is not the complete list. Depending on the parameters r_b, Λ , and M , there are many structures. I will not try to make an exhaustive list of structures in this paper.

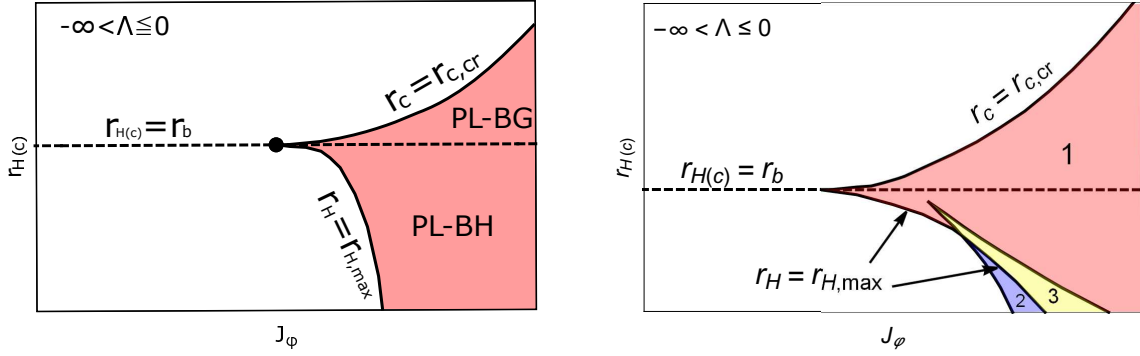


Figure 14: Existence region on $J_\varphi - r_{H(c)}$ plane of Euclidean PL-soliton, PL-BH, and PL-BG instanton when $\Lambda \leq 0$. **(Left)** Simple structure which may appear when both $|\Lambda|/M^2$ and $r_b M$ are large enough. **(Right)** Complicated structure which appear when the condition does not hold. (Examples of parameters that exhibit these structures are $(r_b, \Lambda, M) = (5\sqrt{G}, -0.04/G, 0.3/\sqrt{G})$ **(Left)** and $(r_b, \Lambda, M) = (5\sqrt{G}, -0.004/G, 0.1/\sqrt{G})$ **(Right)**.)

Euclidean PL-soliton, Euclidean PL-BH, and PL-BG instanton

The existence of these geometries also depends on the parameters. Actually, PL-BH and PL-BG are continuously deformable by changing parameters. Therefore, I will treat them in an unified manner.

- $-\infty < \Lambda \leq 0$ (*)

For this case, as shown before, the existence region on the $J_\varphi - r_H$ plane of Euclidean solitons or BHs is below the line $r_H = r_b$ and on the left of the curve $r_H = r_{H,max}(r_b, \Lambda, J_\varphi, M)$. When both $|\Lambda|/M^2$ and $r_b M$ are large enough, that is, when the effect of scalar field is minimum, the existence region of the Euclidean PL-soliton or PL-BH is on the right of the curve $r_H = r_{H,max}(r_b, \Lambda, J_\varphi, M)$ and below $r_H = r_b$, the existence region of the PL-BG instanton is between the line $r_c = r_b$ and the curve $r_c = r_{c,cr}(r_b, \Lambda, J_\varphi, M)$. The number of solutions is always one. See Fig. 14 **(Left)**. When the condition does not hold, the structure becomes complicated as Fig. 14 **(Right)**.

- $0 < \Lambda \leq \frac{1}{r_b}$ (*)

In this case, there exists an upper bound on J_φ for a given $r_{H(c)} < \frac{1}{\sqrt{\Lambda}}$. Additionally, there exist several solutions with the same $r_{H(c)}$ and J_φ , and there are many types of structure of the existence domain depending on r_b and M . Let $r_{c,cr}$ denote the lower boundary of solution regions 2 and 1 in Fig. 12. The simplest example of the existence region is shown schematically in Fig. 15 **(Left)**. This type of structure appears when Λ is sufficiently small compared to $1/r_b^2$ and M . When the condition does not hold, the structure becomes more complicated, for example, as Fig 15 **(Right)**. Another example that shows a more complicated structure is shown in Fig. 16.

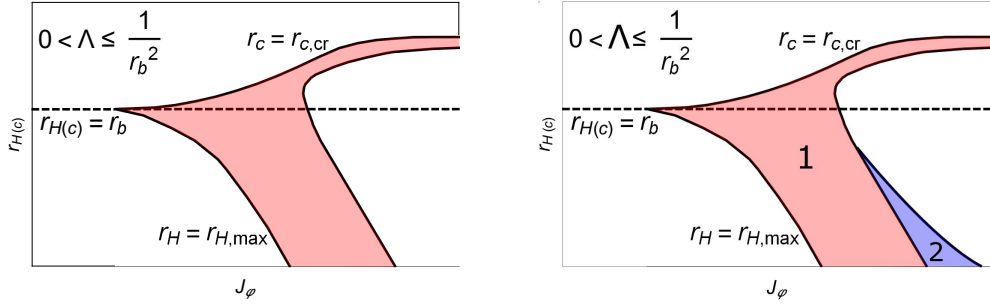


Figure 15: Examples of the structure of existence region on $J_\varphi - r_{H(c)}$ plane of Euclidean PL-soliton, PL-BH, and PL-BG instanton when $0 < \Lambda \leq \frac{1}{r_b^2}$. (**Left**) This type of structure appears when Λ is sufficiently small compared to $1/r_b^2$ and M . This would be the simplest one. (**Right**) When the condition no longer holds, the structure becomes complicated. The numbers in the figures represent the number of solutions with the same r_c and J_φ . (Examples of parameters that exhibit these structures are $(r_b, \Lambda, M) = (5\sqrt{G}, 0.012/G, 0.5/\sqrt{G})$ (**Left**) and $(r_b, \Lambda, M) = (5\sqrt{G}, 0.036/G, 0.5/\sqrt{G})$ (**Right**).)

- $\frac{1}{r_b^2} < \Lambda \leq \frac{3}{r_b^2}$ (*)

In this parameter range, there are no PL-BG instanton solutions and only PL-BHs and PL-solitons exist. There exist the upper bound and the lower bound of J_φ . The lower bound is always greater than 0. It implies that PL type solutions does not exist in the pure gravity system, same as the previous cases. This case also has many types of structure. The simplest structure is shown in Fig. 17 (**Left**) and a example of complicated structure is Fig. 17 (**Right**).

- $\frac{3}{r_b^2} < \Lambda < \infty$

In this parameter range, there are no PL type solutions.

4.2 Thermodynamic potentials and thermodynamic properties

In the previous subsection, I showed the conditions on J_φ for the existence of saddle points, and the dependence on J_φ of the number of saddle points can be classified into some cases depending on Λ . Therefore, in this subsection, I will consider four cases separately, namely, $-\infty < \Lambda \leq 0$, $0 < \Lambda \leq \frac{1}{r_b^2}$, $\frac{1}{r_b^2} < \Lambda \leq \frac{3}{r_b^2}$, and $\frac{3}{r_b^2} < \Lambda < \infty$, and I will discuss the J_φ dependence of thermodynamic potentials

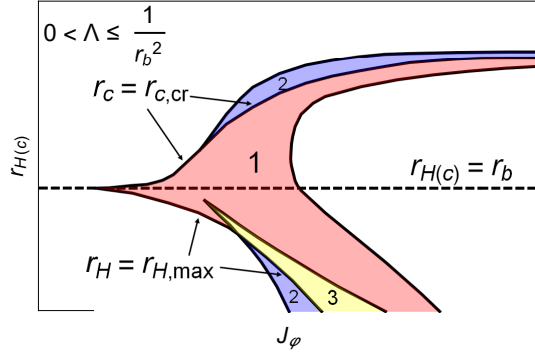


Figure 16: Another example of the structure of existence region on $J_\varphi - r_{H(c)}$ plane of Euclidean PL-soliton, PL-BH, and PL-BG instanton when $0 < \Lambda \leq \frac{1}{r_b^2}$. (A example of parameters that exhibits this structure is $(r_b, \Lambda, M) = (5\sqrt{G}, 0.0012/G, 0.1/\sqrt{G})$.)

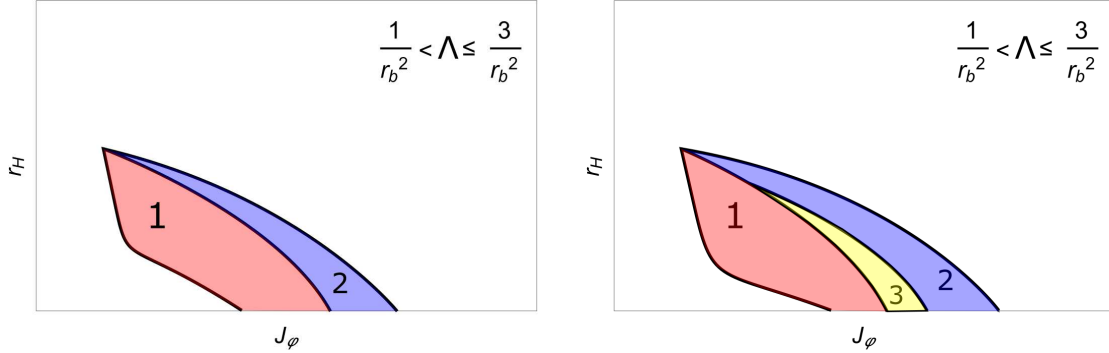


Figure 17: Examples of the structure of existence region on $J_\varphi - r_{H(c)}$ plane of Euclidean PL-soliton and PL-BH when $\frac{1}{r_b^2} < \Lambda \leq \frac{3}{r_b^2}$. Note that this structure is below $r_H = r_b$ line, i.e., there are no PL-BG instanton solutions. **(Left)** Simple structure which may appear when both $|\Lambda|/M^2$ and $r_b M$ are large enough. **(Right)** Complicated structure which appear when the condition does not hold. (Examples of parameters that exhibit these structures are $(r_b, \Lambda, M) = (5\sqrt{G}, 0.044/G, 0.1/\sqrt{G})$ **(Left)** and $(r_b, \Lambda, M) = (5\sqrt{G}, 0.044/G, 0.5/\sqrt{G})$ **(Right)**.)

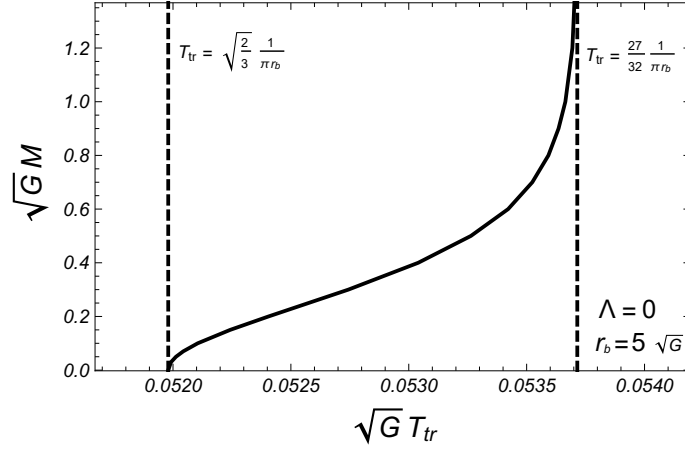


Figure 18: Relation between transition temperature T_{tr} and M with fixing $J_\varphi = \sqrt{\frac{1-\Lambda r_b^2}{4\pi G}} \frac{1}{r_b M}$ when $\Lambda = 0, r_b = 5\sqrt{G}$. As we decrease M , T_{tr} also decreases and T_{tr} reaches the minimal value $\sqrt{\frac{2}{3}} \frac{1}{\pi r_b}$ in the limit $M \rightarrow 0$. For J_φ less than $\sqrt{\frac{1-\Lambda r_b^2}{4\pi G}} \frac{1}{r_b M}$, the transition temperature is placed on the right of the curve and less than $\frac{27}{32\pi r_b}$.

and thermodynamic properties, particularly thermodynamical stability and entropy bound.

4.2.1 $-\infty < \Lambda \leq 0$

- $0 \leq J_\varphi < \sqrt{\frac{1-\Lambda r_b^2}{4\pi G}} \frac{1}{r_b M}$

Only Euclidean BHs (and Euclidean solitons) exist, and their maximum horizon radius is always r_b . The qualitative behaviors of free energy and entropy are almost the same as those for pure gravity with $\Lambda \leq 0$ (see Fig. 3 (Left) or Fig. 4 (Left)); being thermodynamically stable, the system exhibits a Hawking–Page phase transition, and the maximum entropy $\frac{\pi r_b^2}{G}$ is attained at the maximum energy $\frac{r_b}{G} \sqrt{1 - \frac{\Lambda}{3} r_b^2}$. One difference would be that the free energy at low temperature or the ground state energy $E_{gs}(r_b, \Lambda, J_\varphi, M)$ is not zero but some finite value. $E_{gs}(r_b, \Lambda, J_\varphi, M)$ is a monotonically increasing function for J_φ and satisfies $E_{gs}(r_b, \Lambda, 0, M) = 0$ and $E_{gs}(r_b, \Lambda, J_{\varphi, BHcri}(r_b, \Lambda, M), M) = \frac{r_b}{G} \sqrt{1 - \frac{\Lambda}{3} r_b^2}$. For the pure gravity case, the transition temperature depends on $\Lambda \leq 0$ and it takes minimal value $T_{tr} = \frac{27}{32\pi r_b}$ when $\Lambda = 0$. Non-zero J_φ shifts the minimal temperature a little lower. Generally, the larger J_φ , the larger the amount of shift.

Therefore, the lowest transition temperature can be obtained when $J_\varphi = \sqrt{\frac{1-\Lambda r_b^2}{4\pi G}} \frac{1}{r_b M}$ for fixed r_b, Λ, M . Of course, M also affects the amount of the shift. As shown in Fig. 18, the minimal value of the transition temperature will decrease as we decrease M . Therefore, the limiting value of the minimal temperature can be obtained by taking the limit $M \rightarrow 0$ while keeping $J_\varphi = \sqrt{\frac{1-\Lambda r_b^2}{4\pi G}} \frac{1}{r_b M}$. This results in the saddle points becoming those of pure gravity with the positive cosmological

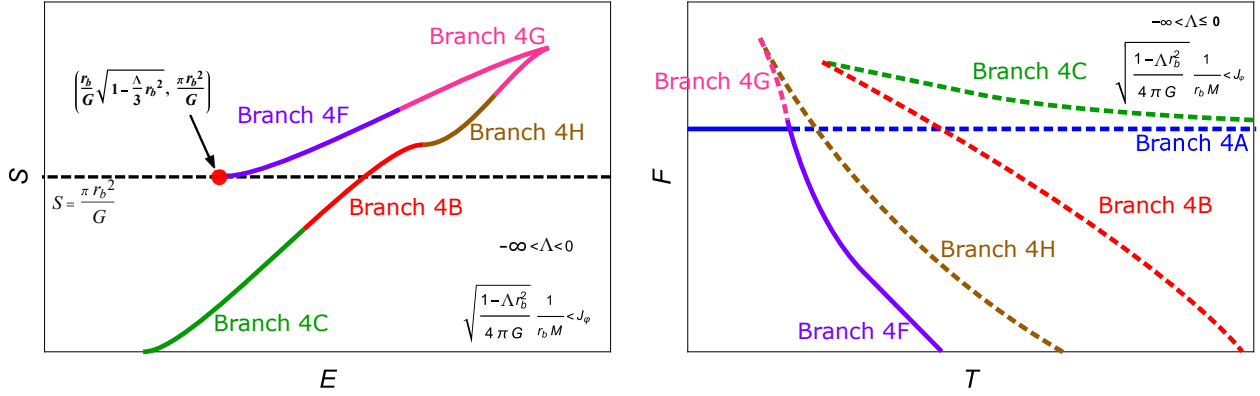


Figure 19: Qualitative behavior of entropies against energy and that of free energy against temperature when $-\infty < \Lambda \leq 0$ and $\sqrt{\frac{1-\Lambda r_b^2}{4\pi G} \frac{1}{r_b M}} \leq J_\varphi$ (and when both $|\Lambda|/M^2$ and $r_b M$ are large enough, or J_φ is enough large). **(Left)** The branches 4B and 4G are thermodynamically stable branches and 4C, 4F, and 4H are thermodynamically unstable ones. 4F and 4G are consist of BG instantons. For 4C, 4B, and 4H, which part of the branches corresponds to which type of solution depends on parameters. **(Right)** At low temperature, branch 4A, which corresponds to Euclidean (PL-)soliton, dominates and, at high temperature, 4F dominates. Therefore, the system is thermodynamically stable at low temperature but unstable at high temperature.

constant $\frac{1}{r_b^2}$, and we can obtain the exact expression

$$T_{tr,mim}(r_b) = \sqrt{\frac{2}{3}} \frac{1}{\pi r_b}, \quad (4.6)$$

which is slightly smaller than $T_{tr} = \frac{27}{32\pi r_b}$. This is the minimum transition temperature of the gravity-scalar system. Note that the transition temperature becomes the minimum one (4.6) for any $\Lambda \leq 0$ when we take the limit $M \rightarrow 0$ while keeping $J_\varphi = \sqrt{\frac{1-\Lambda r_b^2}{4\pi G} \frac{1}{r_b M}}$.

- $\sqrt{\frac{1-\Lambda r_b^2}{4\pi G} \frac{1}{r_b M}} \leq J_\varphi$

In this range, both Euclidean BH, BG instanton and PL type solutions exist. The maximum entropy and energy still exist but are now due to the (PL-)BG instanton. The qualitative behavior of entropies against energy is as shown in Fig. 19 **(Left)**.¹⁸ There are 5 types of branch; the branches 4B and 4G are convex and 4C, 4F, and 4H are concave, i.e., the former correspond to thermodynamically stable branches and the latter to thermodynamically unstable ones. 4F and 4G are consist of BG instantons. For 4C, 4B, and 4H, which part of the branches corresponds to which type of solution depends on parameters. For example, when J_φ is close to $\sqrt{\frac{1-\Lambda r_b^2}{4\pi G} \frac{1}{r_b M}}$, the most part of 4B and 4B consists of Euclidean BHs, the most part of 4H consists of BG instantons, and

¹⁸As I have shown in the previous section, for some parameter, the existence region on $J_\varphi - r_{H(c)}$ plane of PL type solution becomes complicated (Fig. 14 **(Right)**). In that case, the behavior of branch is modified in the low entropy region. However, it does not affect the existence of entropy bound and thermodynamical (in)stability of the system.

the small part near the junction of 4B and 4H consists of PL type solutions. On the other hand, when we choose sufficiently large J_φ , BH solutions cease to exist and 4C, 4B, and 4H consist of only PL type solutions and BG instantons. According to my choice of ground state energy, the energy at the rightmost of the Euclidean BH branch or at the leftmost of 4F is always $\frac{r_b}{G}\sqrt{1 - \frac{\Lambda}{3}r_b^2}$.

The qualitative behavior of free energies is shown in Fig. 19 (**Right**). As we can see, the low temperature region is always dominated by thermodynamically stable branches and it does not suffer from the instability by subdominant unstable branches. In the high temperature region, there always exists the thermodynamically unstable branch 4F and it always gives the dominant contribution. Therefore, at high temperature, the system is thermodynamically unstable.

To summarize, when $\sqrt{\frac{1-\Lambda r_b^2}{4\pi G}} \frac{1}{r_b M} \leq J_\varphi$, the entropy bound still exists and the system is thermodynamically stable at low temperature, but thermodynamically unstable at high temperature. This strange behavior is due to the existence of (PL-)BG instanton.

4.2.2 $0 < \Lambda \leq \frac{1}{r_b^2}$

As I have shown in the previous subsection, the types of BG instanton and PL type solution are numerous and the behavior is complicated when $0 < \Lambda \leq \frac{1}{r_b^2}$, such as in Figs. 12, 13 and 15, 16. Here, I will consider only the case of Fig. 12 and Fig. 15 (**Left**), that is, when Λ/M^2 and $r_b M$ have sufficient magnitude. It is clear that, at least, the additional structures at small horizon radius region in Fig. 15, 16 does not affect the existence of the entropy bound.¹⁹

- $0 < J_\varphi < \sqrt{\frac{1-\Lambda r_b^2}{4\pi G}} \frac{1}{r_b M}$

Both Euclidean BH and BG instanton exist. The qualitative behaviors of entropies and free energies are shown in Fig. 20. The thermodynamically stable branches are 4A, 4B, and 4E, and the unstable ones are 4C and 4D. The entropy and energy of 4D grow indefinitely, so there are no entropy bounds. Although I do not know its implication, the system has an energy gap above $E = \frac{r_b}{G}\sqrt{1 - \frac{\Lambda}{3}r_b^2}$. There are no such energy gaps in the pure gravity case. According to branch 4D, the system is thermodynamically unstable at low temperature; when 4D is dominant, apparently it is unstable, and when 4A is dominant, quantum tunneling may lead to an infinite growth of the cosmological horizon. However, due to 4E, the system is thermodynamically stable at high temperature. The situation is opposite to the case of $-\infty < \Lambda \leq 0$, $\sqrt{\frac{1-\Lambda r_b^2}{4\pi G}} \frac{1}{r_b M} < J_\varphi$, where the system is thermodynamically stable at low temperature and unstable at high temperature. Another property of the system in a thermal bath is the existence of an effective entropy bound; that is, there exists the maximum entropy in thermal equilibrium, $S = \frac{\pi r_b^2}{4G} \left(\sqrt{\frac{12}{\Lambda r_b^2} - 3} - 1 \right)^2$, which can be reached when we take $T \rightarrow \infty$.

- $\sqrt{\frac{1-\Lambda r_b^2}{4\pi G}} \frac{1}{r_b M} < J_\varphi < \infty$

¹⁹I confirmed, by numerical calculation, that it does not affect thermodynamical stability either.

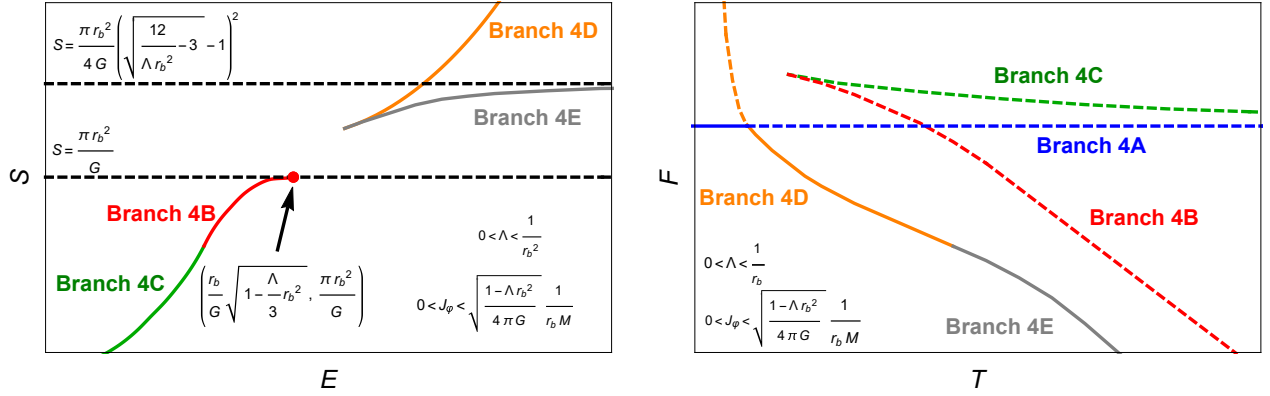


Figure 20: Qualitative behaviors of entropies (left panel) and free energies (right panel) when $0 < \Lambda < \frac{1}{r_b^2}$ and $0 < J_\varphi < \sqrt{\frac{1-\Lambda r_b^2}{4\pi G}} \frac{1}{r_b M}$. Branch 4A is of the Euclidean soliton, branches 4B and 4C are of the Euclidean BH, and branches 4D and 4E are of the BG instanton. **(Left)** The entropy of branch 4D, which is the dominant saddle at high energy, has no bound and increases indefinitely. Unlike that branch, the entropy of 4E has the bound $S = \frac{\pi r_b^2}{4G} \left(\sqrt{\frac{12}{\Lambda r_b^2} - 3} - 1 \right)^2$. **(Right)** The thermodynamically stable branches are 4A, 4B, and 4E. Although 4A dominates at low temperature, it suffers from quantum tunneling to 4D. Therefore, the system is thermodynamically unstable at low temperature. On the other hand, 4E does not suffer from quantum tunneling instabilities.

We have seen there are two types of BG instanton:

- the branch that consists of 4F, 4G, 4H appearing when $-\infty < \Lambda \leq 0, \sqrt{\frac{1-\Lambda r_b^2}{4\pi G}} \frac{1}{r_b M} < J_\varphi < \infty$
- the branch that consists of 4D, 4E appearing when $0 < \Lambda \leq \frac{1}{r_b^2}, 0 < J_\varphi < \sqrt{\frac{1-\Lambda r_b^2}{4\pi G}} \frac{1}{r_b M}$

Roughly, the former causes the instability at high temperature and the latter causes the one at low temperature. In this parameter range, both types exist. As we will see shortly, they make the system thermodynamically unstable for all temperatures. Fig. 21 shows the behaviors of the free energies and entropies of the branch 4F, 4G, 4H, 4D, and 4E. Branch 4A, 4B, and 4C cease to exist above some critical value of J_φ . Even when they exist, it does not give the dominant contribution to the free energy, does not affect the thermodynamical stability, and does not relate to the existence of the entropy bound as we saw before. Therefore, I do not draw it in Fig. 21 (and Fig. 22). From the figure, it is clear that there is no entropy bound. In the right panel of the figure, the low and high temperature regions are dominated by branches 4A and 4E, respectively, which are thermodynamically stable branches. Only the middle temperature region is dominated by the thermodynamically unstable branch 4D. However, both the low and high temperature regions suffer from quantum tunneling instability. Eventually, the system is thermodynamically unstable for all temperature regions. In the figure, the points **a**, **b**, and **c** denote the boundary between 4D and 4E, that between 4G and 4H, and that between 4F and 4G, respectively. As J_φ is increased, these points become closer. At some critical value, which I call $J_{\varphi, BG\text{cri}}(r_b, \Lambda, M)$, these points coincide (i.e., branch 4G disappears). Above that value, branches 4D, 4E, 4F, and 4H are reconnected as in Fig. 22. Branches 4E and 4H are connected, and 4D and 4F are connected. I rename the latter branch

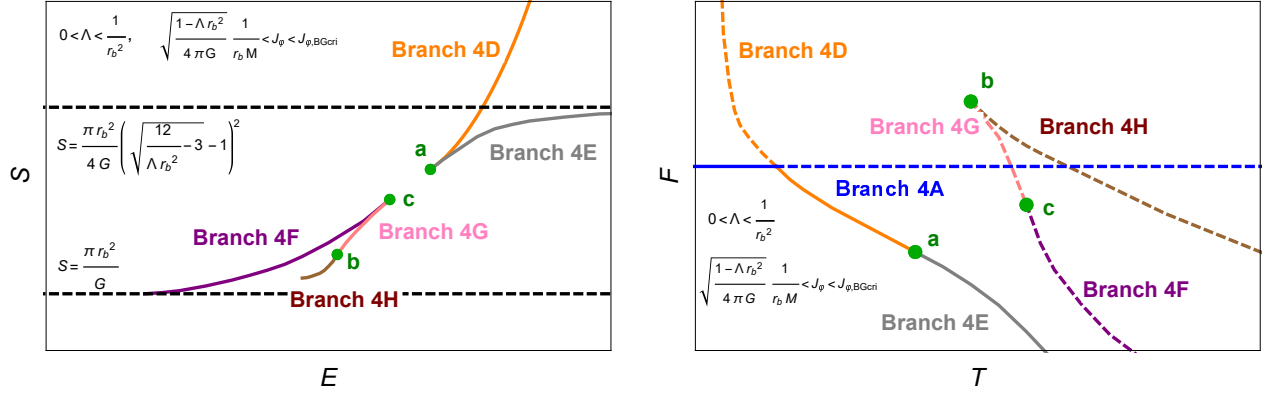


Figure 21: Qualitative behaviors of entropies (left panel) and free energies (right panel) of BG instanton (and Euclidean soliton) when $0 < \Lambda < \frac{1}{r_b^2}$ and $\sqrt{\frac{1-\Lambda r_b^2}{4\pi G}} \frac{1}{r_b M} < J_\varphi < J_{\varphi, BGcri}$. The thermodynamically stable branches are 4A, 4E, and 4G; the others are unstable. As we increase J_φ , the points **a**, **b**, and **c** become close and coincide when J_φ becomes some critical value $J_{\varphi, BGcri}(r_b, \Lambda, M)$. Above that value, the branches are reconnected as in Fig. 22. **(Left)** The dominant saddles are 4F and 4D. There is no entropy bound. **(Right)** Although some temperature regions are dominated by thermodynamically stable branches 4A and 4E, they suffer from quantum tunneling instability. Therefore, the system is thermodynamically unstable.

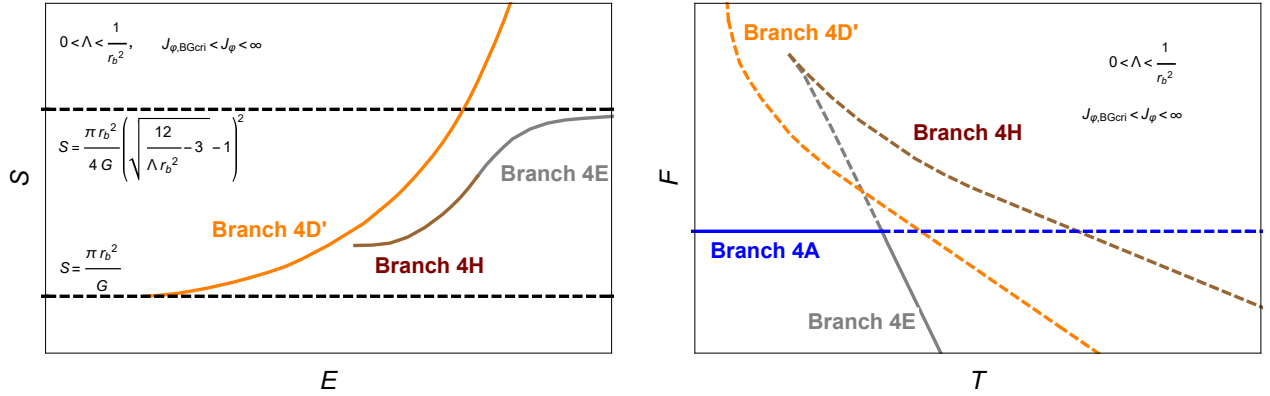


Figure 22: Qualitative behaviors of entropies (left panel) and free energies (right panel) of BG instanton (and Euclidean soliton) when $0 < \Lambda \leq \frac{1}{r_b^2}$ and $J_{\varphi, BGcri}(r_b, \Lambda, M) < J_\varphi < \infty$. The thermodynamically stable branches are 4A and 4E; branches 4D' and 4H are unstable. **(Left)** The dominant saddle is 4D'. There is no entropy bound. **(Right)** Although the dominant saddles are the thermodynamically stable branches 4A and 4E, they suffer from quantum tunneling instability. Therefore, the system is thermodynamically unstable.

4D'. Owing to the existence of 4D', the system has no entropy bound and is thermodynamically unstable.

$$4.2.3 \quad \frac{1}{r_b^2} < \Lambda \leq \frac{3}{r_b^2}$$

When Λ is in this range, the behaviors of free energy and entropy of BG instanton branch are qualitatively the same as in the case of pure gravity with $\frac{1}{r_b^2} < \Lambda$ and branch 4D', that is, there is no entropy bound. Since the free energies of BH branches and PL branches are always subdominant same as before, the system is thermodynamically unstable.

$$4.2.4 \quad \frac{3}{r_b^2} < \Lambda < \infty$$

This is qualitatively the same as the pure gravity case with $\frac{3}{r_b^2} \leq \Lambda$. For any J_φ , the only saddle point is the BG instanton, which is thermodynamically unstable.

5 Discussion

Summary

In this paper, I investigated the thermodynamical properties of the pure gravity system and those of the gravity-scalar system with $S^2 \times \mathbb{R}$ boundary geometry, assuming that all the Euclidean saddle points within minisuperspace (2.11), (2.12) contribute to the path integral. Firstly, I investigated the pure gravity case in section 3. As is known in the literature, the pure gravity system with $\Lambda \leq 0$ has the entropy bound $\frac{\pi r_b^2}{G}$, is thermodynamically stable, and exhibits a Hawking–Page phase transition [4, 5]. Here, r_b is the radius of boundary S^2 . I showed that these properties change drastically when $\Lambda > 0$ due to the contribution of a new type of saddle point geometries, which I call the BG instanton; the system ceases to have an entropy bound and becomes thermodynamically unstable. In section 4, I extended the system by including a scalar field with simple φ^2 potential. I showed that, when $\Lambda \leq 0$ and the boundary value of scalar field J_φ is smaller than the critical value $\sqrt{\frac{1-\Lambda r_b^2}{4\pi G}} \frac{1}{r_b M}$, the system has both an entropy bound and thermodynamical stability. This is because there do not exist BG instantons in this parameter range. However, when $\Lambda > 0$ or when $\sqrt{\frac{1-\Lambda r_b^2}{4\pi G}} \frac{1}{r_b M} < J_\varphi$, BG instantons exist and at least one of the properties is (partially) lost. Precisely, depending on parameters, there can exist two type of BG instanton. The existence of the one makes the system lose the entropy bound and thermodynamical stability at low temperature, and that of the other makes the system lose thermodynamical stability at high temperature. I summarize the thermodynamical properties of the pure gravity system and the scalar-gravity system in Table 1.

Other potentials

Although I consider the simplest potential in this paper, some properties may be common for other potentials. For example, consider a \mathbb{Z}_2 symmetric concave potential. If we assume that the scalar field always decreases toward the bolt or the center, as it does for the φ^2 potential, we can obtain the critical value of J_φ below which the system is thermodynamically stable when $\Lambda \leq 0$ ($\sqrt{\frac{1-\Lambda r_b^2}{4\pi G}} \frac{1}{r_b M}$ for the φ^2 potential case). For example, when $V(\varphi) = \frac{1}{2n} \lambda_{2n} \varphi^{2n}$, the critical value may

	Λ	$(0 \leq) J_\varphi$	Entropy bound	Thermodynamical stability	Transition temperature T_{tr}
Pure gravity	$\Lambda \leq 0$	N/A	$\frac{\pi r_b^2}{G}$	stable	$\frac{27}{32\pi r_b} \leq T_{tr} < \frac{1}{\pi r_b}$
	$0 < \Lambda$	N/A	none	unstable	N/A
Gravity	$\Lambda \leq 0$	$J_\varphi \leq \sqrt{\frac{1-\Lambda r_b^2}{4\pi G}} \frac{1}{r_b M}$	$\frac{\pi r_b^2}{G}$	stable	$\sqrt{\frac{2}{3}} \frac{1}{\pi r_b} < T_{tr} < \frac{1}{\pi r_b}$
		$\sqrt{\frac{1-\Lambda r_b^2}{4\pi G}} \frac{1}{r_b M} < J_\varphi$	$\frac{\pi r_{c,max}^2}{G} \left(> \frac{\pi r_b^2}{G} \right)$	low T : stable high T : unstable	N/A
-scalar	$0 < \Lambda \leq \frac{1}{r_b^2}$	$J_\varphi \leq \sqrt{\frac{1-\Lambda r_b^2}{4\pi G}} \frac{1}{r_b M}$	none	low T : unstable high T : stable	N/A
		$\sqrt{\frac{1-\Lambda r_b^2}{4\pi G}} \frac{1}{r_b M} < J_\varphi$	none	unstable	N/A
	$\frac{1}{r_b^2} < \Lambda$	$0 \leq J_\varphi$	none	unstable	N/A

Table 1: Summary of thermodynamical properties of pure gravity system and gravity-scalar system. The definitions of $J_{\varphi, BHcri} = J_{\varphi, BHcri}(r_b, \Lambda, M)$ and $r_{c,max} = r_{c,max}(r_b, J_\varphi, \Lambda, M)$ are written somewhere in section 4. Note that, by symmetry, we can restrict J_φ to non-negative value.

be $J_\varphi = \left(\frac{n(1-\Lambda r_b^2)}{4\pi G \lambda_{2n} r_b^2} \right)^{\frac{1}{2n}}$. We can also say that the minimal transition temperature is $T_{tr} = \sqrt{\frac{2}{3}} \frac{1}{\pi r_b}$, irrelevant of the details of the potential as long as it is \mathbb{Z}_2 symmetric and concave. This may be obtained by taking the limit of parameters of the potential so that it becomes flat, keeping J_φ equal to the critical value. Of course, in order to check these matter, more detailed investigations are needed.

Another direction would be to consider double well type potentials, with false and true vacuums. For definiteness, let the true vacuum be a negative value and the false vacuum be a positive value, and let the potential form be suitable for thin-wall approximation. When we choose J_φ as the true vacuum, there are two types of solution: one is the same as the solution in pure gravity with $\Lambda < 0$, and the other is constructed from the $\Lambda < 0$ solution, the $\Lambda > 0$ solution, and a thin wall. The thermodynamical properties of the system would be different from the ones considered in this paper, and it is enough simple to analyze the detail. This will be left for future study.

Gravity-Maxwell system

There exist BG instantons also in the gravity-Maxwell system. Consider a Reissner–Nordstrom BH solution and let r_{in} be the radius of the inner horizon and r_b be some radius smaller than r_{in} . If we Euclideanize the $[r_b, r_{in}]$ region with an appropriate circumference, we obtain a BG instanton. Although the thermodynamics of the gravity-Maxwell system was previously investigated in [42, 43, 44, 45], the effect of a BG instanton was not considered. It would be interesting to consider its effect and see how its thermodynamical properties are modified.

Integration contour problem

In this paper, I assumed that all Euclidean saddle points contribute to the partition function. This assumption leads to the inclusion of BG instantons in the path integral and makes the system thermodynamically unstable for some cases. However, as shown in [21], in order to define the Euclidean gravitational path integral, its contour must be purely complex. Therefore, some Euclidean saddles may not contribute and some complex saddles may contribute to the path integral. Following the principle of [22], I have to check whether there exist one or more steepest descent contours passing through all Euclidean saddles shown in this paper. I also have to check, if they pass through complex saddles, whether they do not change the thermodynamical properties. These issues will be investigated in [33] for the pure gravity case.

Acknowledgement

The author is grateful to Shintaro Sato for useful discussion. This work was supported in part by the Waseda University Grant for Special Research Project (No. 2020C-775).

A Numerical solutions in the gravity-scalar system

In this Appendix, I explicitly show some numerical solutions of the gravity-scalar system. The equation of motion of the system (2.9) is given by

$$G_{\mu\nu} + \Lambda g_{\mu\nu} = 8\pi G T_{\mu\nu} \quad (\text{A.1})$$

$$(\square - M^2)\varphi = 0 \quad (\text{A.2})$$

where the energy momentum tensor is given by

$$T_{\mu\nu} = \frac{2}{\sqrt{g}} \frac{\delta I_{c,scalar}^E}{\delta g^{\mu\nu}} = \partial_\mu \varphi \partial_\nu \varphi - \frac{1}{2} g_{\mu\nu} (g^{\alpha\beta} \partial_\alpha \varphi \partial_\beta \varphi + M^2 \varphi^2) \quad (\text{A.3})$$

Substituting the ansatz (4.2) into the above equation, we obtain the following basic equations:

$$\begin{aligned} \delta' &= -4\pi G r (\varphi')^2 \\ f' + \frac{f - 1 + \Lambda r^2}{r} &= -4\pi G r [f(\varphi')^2 + M^2 \varphi^2] \\ -f \delta' \varphi' + \frac{2}{r} f \varphi' + f' \varphi' + f \varphi'' - M^2 \varphi &= 0 \end{aligned} \quad (\text{A.4})$$

There are three types of solutions: Euclidean soliton, Euclidean BH, and BG instanton. I will explain the boundary conditions and show numerical solutions separately.

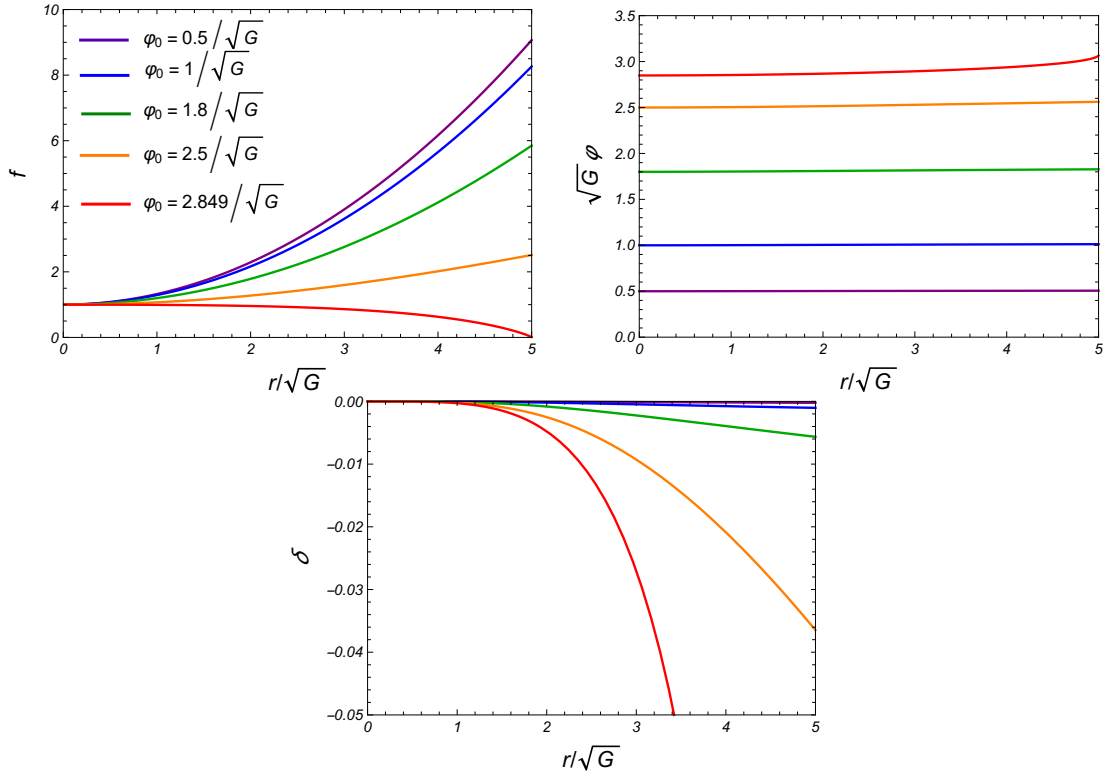


Figure 23: Solutions f, φ, δ of Euclidean soliton when φ_0 is $0.5/\sqrt{G}, 1/\sqrt{G}, 1.8/\sqrt{G}, 2.5/\sqrt{G}$, and $2.849/\sqrt{G}$ ($r_b = 5\sqrt{G}, \Lambda = -0.04/G, M = 0.1/\sqrt{G}$).

A.1 Euclidean soliton

For a solitonic solution, the functions must behave as follows near the center $r = 0$ for regularity:

$$\delta(r) = -\frac{\pi GM^4 \varphi_0^2}{9} r^4 + \dots \quad (\text{A.5})$$

$$f(r) = 1 - \frac{\Lambda + 4\pi GM^2 \varphi_0^2}{3} r^2 + \dots \quad (\text{A.6})$$

$$\varphi(r) = \varphi_0 + \frac{M^2}{6} \varphi_0 r^2 + \dots \quad (\text{A.7})$$

where φ_0 is a shooting parameter that must be chosen for the functions to satisfy desired boundary conditions at $r = r_b$:

$$\varphi(r_b) = J_\varphi \quad (\text{A.8})$$

Note that I set $\delta(0) = 0$ using the freedom of rescaling the time coordinate. Examples of the solutions are shown in Fig. 23.

$\varphi(r)$ always increases toward the boundary from the center, and $f(r_b)$ decreases as we increase φ_0 . The limiting case where $f(r_b)$ goes to zero will be discussed in A.4.

A.2 Euclidean BH

Let the radius of the bolt (horizon) be $r_H < r_b$ where $f(r)$ is zero. The functions must behave as follows near the bolt for regularity:

$$\delta(r) = -4\pi Gr_H \left(\frac{r_H M^2 \varphi_H}{1 - \Lambda r_H^2 - 4\pi Gr_H^2 M^2 \varphi_H^2} \right)^2 (r - r_H) + \dots \quad (\text{A.9})$$

$$f(r) = \frac{1 - \Lambda r_H^2 - 4\pi Gr_H^2 M^2 \varphi_H^2}{r_H} (r - r_H) + \dots \quad (\text{A.10})$$

$$\varphi(r) = \varphi_H + \frac{r_H M^2 \varphi_H}{1 - \Lambda r_H^2 - 4\pi Gr_H^2 M^2 \varphi_H^2} (r - r_H) + \dots \quad (\text{A.11})$$

where φ_H is a shooting parameter. Therefore, there are two shooting parameters $\{r_H, \varphi_H\}$, and they must be chosen for the functions to satisfy desired boundary conditions at $r = r_b$:

$$\frac{4\pi}{f'(r_H)} \sqrt{f(r_b)} e^{-\delta(r_b)} = \beta \quad (\text{A.12})$$

$$\varphi(r_b) = J_\varphi \quad (\text{A.13})$$

I set $\delta(r_H) = 0$ using the freedom of rescaling the time coordinate. When we fix r_H and vary φ_0 , the behaviors of solutions are similar to those in the Euclidean soliton case (Fig. 23). In Fig. 24, I show the behavior of solutions with varying r_H but fixing J_φ to a value less than $\sqrt{\frac{1 - \Lambda r_b^2}{4\pi G} \frac{1}{r_b M}}$. In this case, the horizon radius can take any value in $(0, r_b)$. In Fig. 25, I show the behavior of solutions with varying r_H but this time fixing J_φ to a value greater than $\sqrt{\frac{1 - \Lambda r_b^2}{4\pi G} \frac{1}{r_b M}}$. As we increase the horizon radius, $f(r_b)$ goes to zero. Therefore, there exists the maximum horizon radius $r_{H,max}(r_b, \Lambda, J_\varphi, M)$. This limiting case will be discussed in A.4.

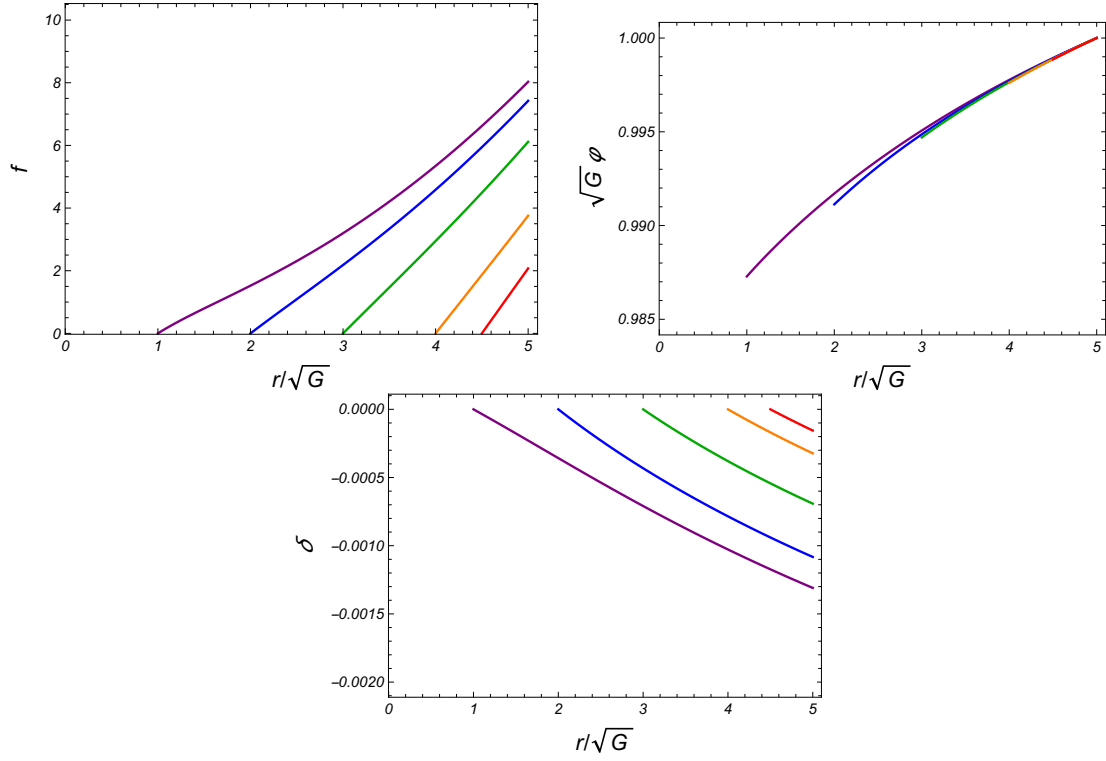


Figure 24: Solutions f, φ, δ of Euclidean BH when r_H is $\sqrt{G}, 2\sqrt{G}, 3\sqrt{G}, 4\sqrt{G}$, and $4.5\sqrt{G}$. φ_H is chosen so that $J_\varphi = 1/\sqrt{G} < \sqrt{\frac{1-\Lambda r_b^2}{4\pi G}} \frac{1}{r_b M}$ ($r_b = 5\sqrt{G}, \Lambda = -0.04/G, M = 0.1/\sqrt{G}$).

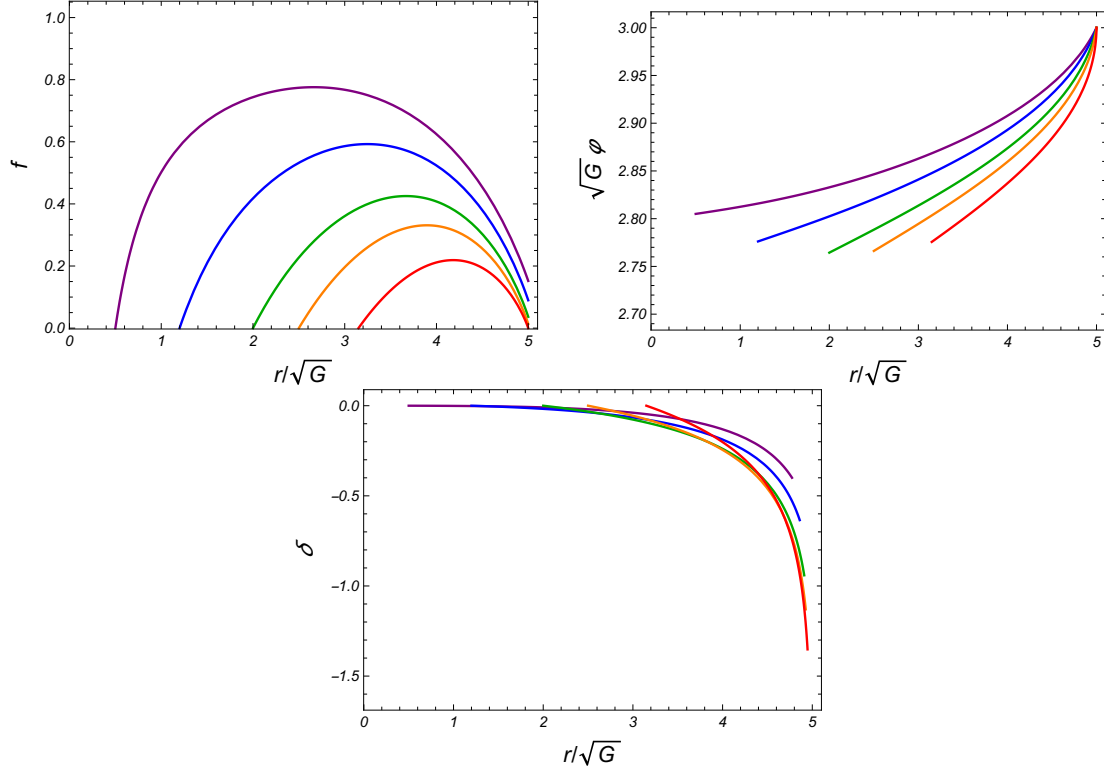


Figure 25: Solutions f, φ, δ of Euclidean BH when r_H is $0.5\sqrt{G}, 1.2\sqrt{G}, 2\sqrt{G}, 2.5\sqrt{G}$, and $3.15\sqrt{G}$. φ_H is chosen so that $J_\varphi = 3/\sqrt{G} > \sqrt{\frac{1-\Lambda r_b^2}{4\pi G}} \frac{1}{r_b M}$. ($r_b = 5\sqrt{G}, \Lambda = -0.04/G, M = 0.1/\sqrt{G}$) The maximum radius is $r_{H,max}(5\sqrt{G}, -0.04/G, 3/\sqrt{G}, 0.1/\sqrt{G}) \simeq 3.15\sqrt{G}$.

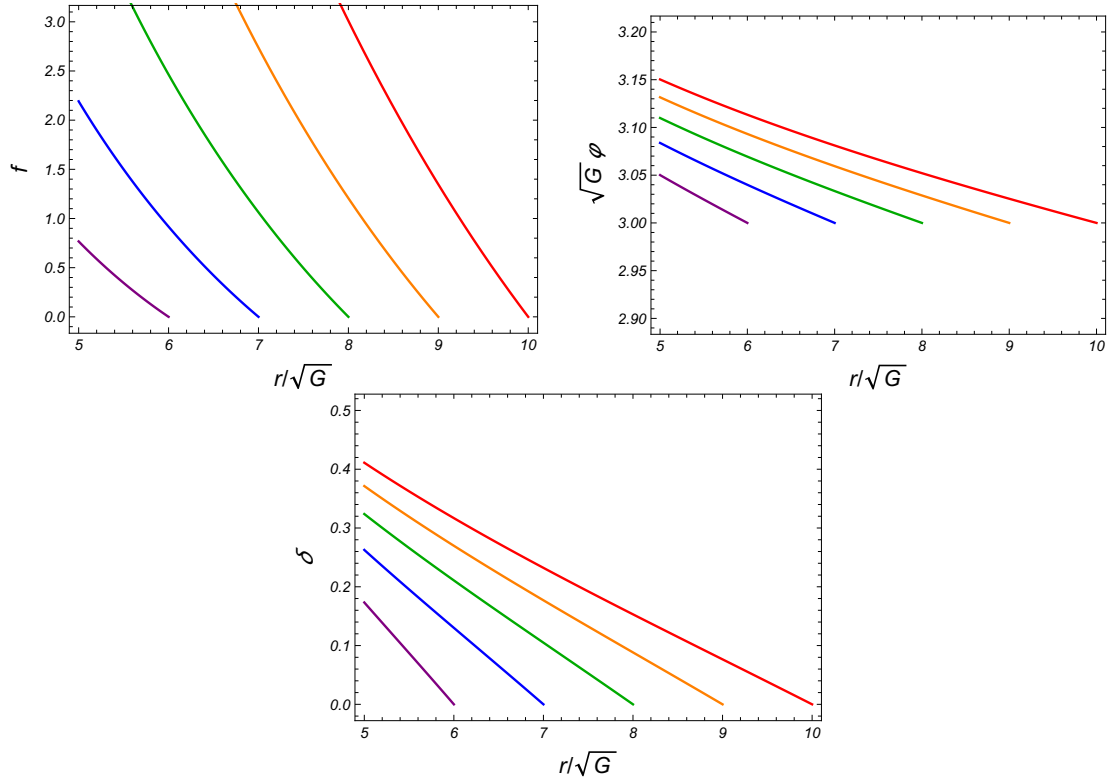


Figure 26: Solutions f, φ, δ of BG instanton when r_c is $6\sqrt{G}, 7\sqrt{G}, 8\sqrt{G}, 9\sqrt{G}$, and $10\sqrt{G}$. φ_H is set to $3/\sqrt{G}$ ($r_b = 5\sqrt{G}, \Lambda = -0.04/G, M = 0.1/\sqrt{G}$).

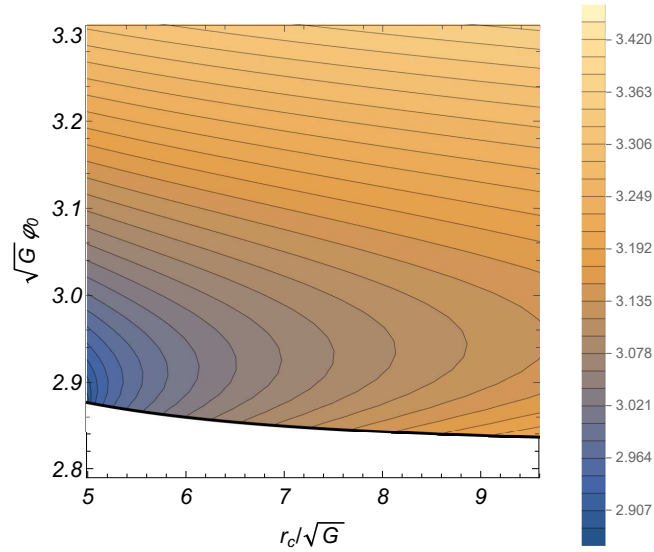


Figure 27: Contour plot on $r_c - \varphi_0$ plane. The height represents the value of J_φ ($r_b = 5\sqrt{G}, \Lambda = -0.04/G, M = 0.1/\sqrt{G}$).

A.3 BG instanton

Let the radius of the bolt (cosmological horizon) be $r_c > r_b$ where $f(r)$ is zero. The functions must behave as follows near the bolt for regularity:

$$\delta(r) = -4\pi G r_c \left(\frac{r_c M^2 \varphi_c}{1 - \Lambda r_c^2 - 4\pi G r_c^2 M^2 \varphi_c^2} \right)^2 (r - r_c) + \dots \quad (\text{A.14})$$

$$f(r) = \frac{1 - \Lambda r_c^2 - 4\pi G r_c^2 M^2 \varphi_c^2}{r_c} (r - r_c) + \dots \quad (\text{A.15})$$

$$\varphi(r) = \varphi_c + \frac{r_c M^2 \varphi_c}{1 - \Lambda r_c^2 - 4\pi G r_c^2 M^2 \varphi_c^2} (r - r_c) + \dots \quad (\text{A.16})$$

As in the Euclidean BH case, there are two shooting parameters $\{r_c, \varphi_c\}$, and they must be chosen for the functions to satisfy desired boundary conditions at $r = r_b$:

$$-\frac{4\pi}{f'(r_c)} \sqrt{f(r_b)} e^{-\delta(r_b)} = \beta \quad (\text{A.17})$$

$$\varphi(r_b) = J_\varphi \quad (\text{A.18})$$

I set $\delta(r_c) = 0$ as before. Examples of the solutions are shown in Fig. 26.

In subsection 4.1, I characterized BG instantons by $\{r_c, J_\varphi\}$ in order to see the connection to boundary quantities. However, these parameters are not good for parameterizing BG instantons. Instead, we can use $\{r_c, \varphi_0\}$ for parameterization. Fig. 27 shows a contour plot on the $r_c - \varphi_0$ plane, where the height represents the value of J_φ . The black curve represents $\varphi_0 = \sqrt{\frac{1 - \Lambda r_c^2}{4\pi G}} \frac{1}{r_c M}$, below which no BG instantons exist.

Note that Fig. 27 is for $\Lambda < 0$, and the situation is more complicated for $\Lambda > 0$.

A.4 PL type solution

When I obtained Euclidean soliton or Euclidean BH solutions, what I practically did is to solve the equation motion from the center or the bolt to the outward, then stop the integration at some radius r_b . If we do not stop integration, it eventually hits the point where $f(r) = 0$ (See Fig. 23, 25). If we recall the behavior of $f(r)$ of (Euclidean) dS or Schwarzschild dS solution, it may seem an analog of cosmological horizon. However, this is not the case. Let r_{max} be the radius of the point $f(r) = 0$, other than the radius of bolt when we consider Euclidean BH. Near r_{max} , the solutions may behave as follows;

$$\varphi(r) \simeq \varphi_{max} - \frac{1}{\sqrt{2\pi G r_{max}}} (r_{max} - r)^{\frac{1}{2}} \quad (\text{A.19})$$

$$f(r) \simeq \left(8\pi G r_{max} M^2 \varphi_{max}^2 - \frac{2}{r_b} (1 - \Lambda r_{max}^2) \right) (r_{max} - r) \quad (\text{A.20})$$

$$\delta(r) \simeq \delta_{max} + \frac{1}{2} \log(r_{max} - r) \quad (\text{A.21})$$

where φ_{max} and δ_{max} are some constants. The solution with $r_H = 3.15\sqrt{G}$ in Fig. 25 is close to the above solution. Although $f(r)$ goes to zero, the geometry is not cupped off at r_{max} because the

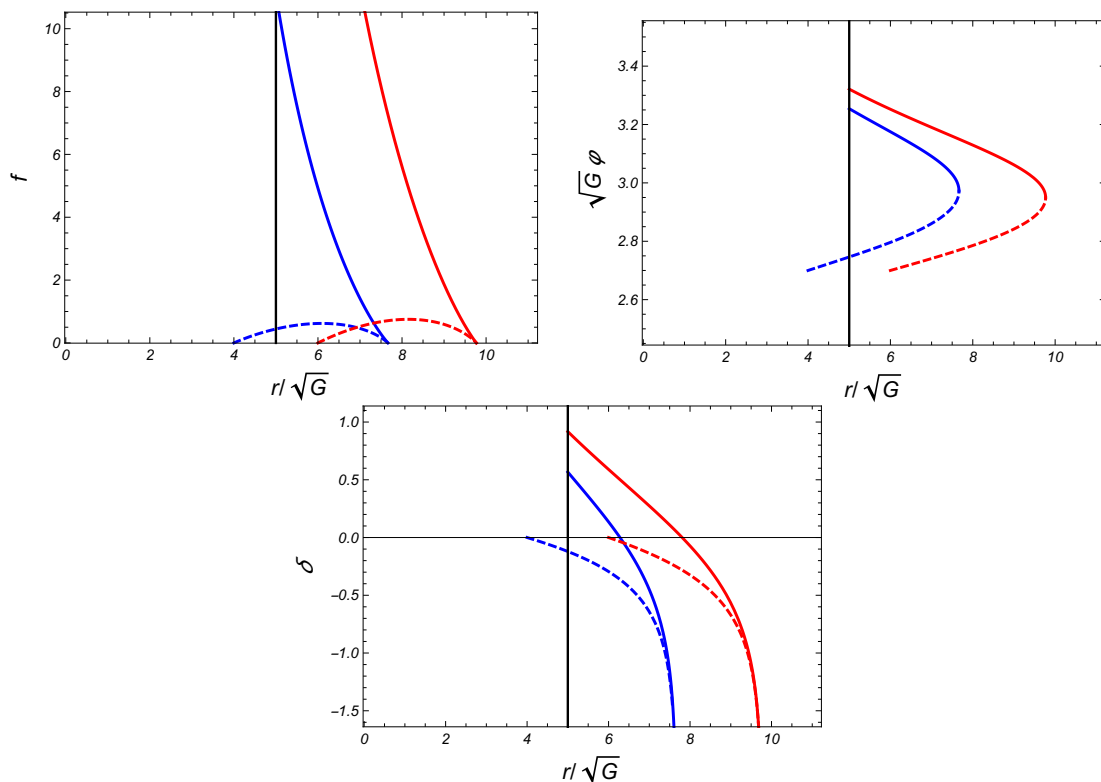


Figure 28: Solutions f, φ, δ of Euclidean PL-BH and PL-BG instanton when $r_H = 4\sqrt{G}, \varphi_H = 2.7\sqrt{G}$ for the former and $r_H = 6\sqrt{G}, \varphi_H = 2.7\sqrt{G}$ for the latter. The vertical line represents the position of the boundary. $r_{max} \simeq 7.665\sqrt{G}$ for the former and $r_{max} \simeq 9.769\sqrt{G}$ for the latter. ($r_b = 5\sqrt{G}, \Lambda = -0.04/G, M = 0.1/\sqrt{G}$)

tt component of the metric stay finite $e^{-2\delta(r)} f(r) \simeq const.$ there. Therefore, if we use a suitable coordinate, we can extend the solution further and the resulting solution becomes the one shown in Fig. 9. The examples of Euclidean PL-BH and PL-BG instanton are shown in Fig. 28.

References

- [1] J. M. Bardeen, B. Carter, and S. W. Hawking, Commun. Math. Phys. **31** (1973) 161
- [2] S. W. Hawking, Commun. Math. Phys. **43** (1975) 199
- [3] G. W. Gibbons and S. W. Hawking, Phys. Rev. D **15** (1977) 1082
- [4] S. W. Hawking and D. N. Page, Commun. Math. Phys. **87** (1983) 577
- [5] J. W. York, Jr., Phys. Rev. D **33** (1986) 2092
- [6] J. D. Brown, J. Creighton, and R. B. Mann, Phys. Rev. D **50** (1994) 6394

- [7] G. 't Hooft , Conf. Proc. C 930308 (1993) 284
- [8] L. Susskind , J. Math. Phys. **36** (1995) 637
- [9] R. B. Mann , Phys. Rev. D **60** (1999) 104047
- [10] S. Miyashita , arXiv: 2007.13294 (2020)
- [11] P. Kraus, F. Larsen, and R. Siebelink , Nucl. Phys. B **563** (1999) 259
- [12] J. D. Brown, G. L. Comer, E. A. Martinez, J. Melmed, B. F. Whiting and J. W. York, Jr. , Class. Quant. Grav. **7** (1990) 1433
- [13] H. W. Braden, B. F. Whiting, and J. W. York, Jr. , Phys. Rev. D **36** (1987) 3614
- [14] J. J. Halliwell and J. Louko , Phys. Rev. D **42** (1990) 3997
- [15] J. Louko and B. F. Whiting , Class. Quant. Grav. **9** (1992) 457
- [16] J. Memled and B. F. Whiting , Phys. Rev. D **49** (1994) 907
- [17] S. Miyashita , Class. Quant. Grav. **36** (2019) 155003
- [18] A. Di Tucci, M. P. Heller, and J.-L. Lehners , arXiv:2007.04872 (2020)
- [19] J. D. Brown and J. W. York, Jr. , Phys. Rev. D **47** (1993) 1407
- [20] S. W. Hawking and S. F. Ross , Phys. Rev. D **52** (1995) 5865
- [21] G. W. Gibbons , S. W. Hawking, and M. J. Perry , Nucl. Phys. B **138** (1978) 141
- [22] J. J. Halliwell and J. B. Hartle , Phys. Rev. D **41** (1990) 1815
- [23] B. Wang and C. G. Huang , Mod. Phys. Lett. A **16** (2001) 1487
- [24] C. G. Huang, L. Liu, and B. Wang , Phys. Rev. D **65** (2002) 083501
- [25] M. H. Dehghani , Phys. Rev. D **65** (2002) 104030
- [26] Y. Sekiwa , Phys. Rev. D **73** (2006) 084009
- [27] H. Saida , Prog. Theor. Phys. **122** (2010) 1239
- [28] D. Kubiznak and F. Simovic , Class.Quant.Grav. **33** (2016) 24, 245001
- [29] G. W. Gibbons and S. W. Hawking , Commun. Math. Phys. **66** (1979) 291
- [30] A. Almheiri, R. Mahajan, J. Maldacena, and Y. Zhao , JHEP **03** (2020) 149
- [31] R. G. Cai, Y. S. Myung, and Y. Z. Zhang , Phys. Rev. D **65** (2002) 084019
- [32] D. J. Gross, M. J. Perry, and L. G. Yaffe , Phys. Rev. D **25** (1982) 330
- [33] S. Miyashita, “Partition Functions for Gravitational Thermodynamics,” *work in progress*

- [34] D. Kastor, S. Ray, and J. Traschen , *Class. Quant. Grav.* **26** (2009) 195011
- [35] M. Cvetič, G. W. Gibbons, D. Kubiznak, and C. N. Pope , *Phys. Rev. D***84** (2011) 024037
- [36] A. R. Brown, H. Gharibyan, G. Penington, and L. Susskind , *JHEP* **08** (2020) 121
- [37] J. W. York, Jr. , *Phys. Rev. Lett.* **28** (1972) 1082
- [38] J. D. Brown and J. W. York, Jr. , *Phys. Rev. D* **47** (1993) 1420
- [39] J. M. Maldacena, *Int. J. Theor. Phys.* 38 (1999) 1113, *Adv. Theor. Math. Phys.* **2** (1998) 231
- [40] S. S. Gubser, I. R. Klebanov, and A. M. Polyakov , *Phys. Lett. B* **428** (1998) 105
- [41] E. Witten , *Adv. Theor. Math. Phys.* **2** (1998) 253
- [42] H. W. Braden, J. D. Brown, B. F. Whiting, and J. W. York, Jr. , *Phys. Rev. D***42** (1990) 3376
- [43] S. Carlip and S. Vaidya, *Class. Quant. Grav.* **20** (2003) 3827
- [44] A. P. Lundgren , *Phys. Rev. D***77** (2008) 044014
- [45] P. Basu, C. Krishnan, and P. N. Bala Subramanian , *JHEP* **11** (2016) 041